





# LIBRARY Michigan State University

This is to certify that the

#### thesis entitled

# EXPERIMENTAL INVESTIGATION OF TUNED CENTRIFUGAL PENDULUM VIBRATION ABSORBERS

presented by

Yi Wu

has been acce	epted towards fulfillment
of the	requirements for
MS	Mechanical Engineering
	_degree in

Major professor

Date 5/9/00

MSU is an Affirmative Action/Equal Opportunity Institution

**O**-7639

# PLACE IN RETURN BOX to remove this checkout from your record. TO AVOID FINES return on or before date due. MAY BE RECALLED with earlier due date if requested.

DATE DUE	DATE DUE	DATE DUE

11/00 c:/CIRC/DateDue.p65-p.14

# EXPERIMENTAL INVESTIGATION OF TUNED CENTRIFUGAL PENDULUM VIBRATION ABSORBERS

By

Yi Wu

#### **A THESIS**

Submitted to
Michigan State University
in partial fulfillment of the requirement
for the degree of

**MASTER OF SCIENCE** 

Department of Mechanical Engineering

2000

#### **ABSTRACT**

# EXPERIMENTAL INVESTIGATION OF TUNED CENTRIFUGAL PENDULUM VIBRATION ABSORBERS

By

#### Yi Wu

This work addresses the dynamics of the centrifugal pendulum vibration absorber (CPVA). The main thrust of the work concentrates on an experimental investigation of the behavior of a rotating system with two attached pendulums acting as the torsional vibration absorbers. Particular experiments are developed and executed to study the influence of varying the tuning of the absorber, the torque level, the torque frequency, and the mean spin rate. Large absorber motions are allowed and nonlinear behaviors are observed. Results from the experiments are compared to theoretical predictions obtained from previously published works. Particular attention is given to a careful documentation of the parameter values of the experimental system and how they relate to the non-dimensional terms used in the theoretical work. Discrepancies between the theory and the experiments are thoroughly investigated.

To my wife Xiaojia

#### **ACKNOWLEDGMENTS**

Very special thanks to my wife Xiaojia, whose support is unmatched. To my parents and my brother who encouraged me to study in America. Home will always be with you.

Thanks to Dr. Alan Haddow and Dr. Steven Shaw for inviting me to work with them on the research leading to this thesis. Their patience, insight and expertise have made for a great experience. To the faculty and staff at Michigan State University, especially in the Department of Mechanical Engineering. To Mark Berry who helped me a lot doing the experiments. To Reimund Keiser (1998) who set up the experimental facility and to Boon Keat who built the motor mean speed controller.

### **TABLE OF CONTENTS**

LI	ST OF TABLES						vi
LI	ST OF FIGURES						vii
CI	IAPTER						
1.	INTRODUCTION						1
	1.1 History of Vibration Absorber	•			•		3
	1.2 Objectives and Thesis Organization	•	•	•	•	•	3
2.	THEORETICAL REVIEW AND NUM	MERIC	CAL EX	AMPL	ES		5
	2.1 Spring-Mass Absorber .	•		•	•		6
	2.2 Torsional Vibration Absorber	•	•	•	•		10
	2.2.1 Modeling of a Centrifugal Per	ndulum	Vibrati	on Abs	orber (C	CPVA)	10
	2.2.1.1 The Undamped Absorber	•	•		•	•	14
	2.2.1.2 The Damped Absorber	•				•	18
	2.2.2 3-Degree Of Freedom CPVA			•	•		20
	2.2.2.1 The Undamped Absorber	•	•	•	•	•	22
	2.2.2.2 The Damped Absorber	•		•	•		25
	2.2.3 Equations for a CPVA Movin	g Alon	g a Gen	eral Pat	h		27
	2.2.3.1 Analytical Results.	•	•	•	•		32
	2.2.3.2 Numerical Examples	•	•	•	•	•	35
3.	EXPERIMENTAL SETUP						39
	3.1 Experiment Facility	•	•	•	•	•	39
	3.2 Motor Mean Speed Controller	•	•	•	•	•	42
4.	EXPERIMENT RESULTS						43
	4.1 System Parameters	•		•	•	•	43
	4.2 CPVA System Frequency Response	Experi	ments		•	•	46
	4.2.1 System Frequency Response			rs are lo	cked		46
	4.2.1.1 Results	•	•	•	•		46
	4.2.1.2 Discussion.	•			•		46
	4.2.2 Linear System Frequency Res	sponse '	when A	bsorber	s are Fr	ree	47
	4.2.2.1 Results			•	•		48
	4.2.2.2 Discussion.	•		•	•		48
	4.2.3 System Frequency Response	at Diffe	erent To	rque Le	vels	•	49
	4.2.3.1 Results	•	•	•	•	٠	49
	4.2.3.2 Discussion.	•	•	•		•	50
	4.2.4 System Frequency Response					eeds	50
	4.2.4.1 Results					•	51

	4.2.4.2	Discussion.	•	•	•	•	•		51
	4.2.5 Syst	em Frequency F	Respon	se with	Differe	nt Abso	rber Co	rd Len	gth 52
	4.2.5.1	Results .		•			•	•	52
	4.2.5.2	Discussion.	•	•		•		•	53
	4.3 CPVA Bifu	rcation and Mis	tuning	Experin	nents		•	•	54
		ked Absorbers	_	•			•		54
	4.3.2 Bifu	rcation Experim	nent	•		•			55
		Results .	•	•					55
	4.3.2.2	Discussion.	•	•				•	56
	4.3.3 Bifu	rcation Experim	ents b	y Mistu	ning				57
	4.3.3.1	Results .	•	•			•		58
5.	CONCLUDIN FUTURE WO		AND 1	RECON	<b>MEN</b>	DATIO	NS FO	R	59
ΑJ	PPENDICES								61
	APPENDIX A	Linear Torsion	al Vib	ration A	bsorbe	•	•	•	62
	APPENDIX B	Procedure to S	tart-up	the CP	VA Exp	erimen	t.		64
	APPENDIX C	<b>CPVA Experim</b>	ent De	vices C	alibration	on .		•	66
	APPENDIX D	Discussion of	the CP	VA Ord	er.	•	•	•	69
ΒI	BLIOGRAPHY	?							74

## LIST OF TABLES

4.1 CPVA notation and system par	rameter	s values	s.				44
4.2 Relationship between the actua	al physi	ical vari	ables a	nd their	non-dir	nension	al
counterparts		•				•	45
C.1 Experiment result conversion	•	•	•	•	•	•	68
D.1 Estimated CPVA order for different motor mean speed.							70
D.2 Estimated CPVA order with d	•		71				

## **LIST OF FIGURES**

2.1	Spring-mass absorber			•	6
2.2	Normalized amplitude of the main mass and that of the a	bsorbe	r mass	vs.	
	dimensionless frequency, $\omega/\omega_a$			•	9
2.3	Centrifugal Pendulum Vibration Absorber			•	11
	Free body diagram of CPVA				11
	Undamped CPVA frequency response plots (a) $\theta_0/T$ vs. $\alpha$	and (t	o)φ <sub>0</sub> / <i>T</i> ν		16
	Undamped CPVA frequency response plots (a) $\ddot{\theta}/T$ vs. $\alpha$				17
	Frequency response of flywheel acceleration, $\ddot{\theta}/T$ vs. $\omega$ ,				
2.,	damping ratio: 0.0, 0.02, 0.05 and 0.10	ioi dii	iciciit		19
2.8	3-DOF CPVA				20
	Frequency response of rotor acceleration over applied va	rying t	orque.		
	$\ddot{\alpha}/T$ vs. $\omega$			•	23
2.10	Frequency response of rotor acceleration over applied va	arying	torque,		
	$\ddot{\alpha}/T$ vs. $\omega$ , for different coupler stiffnesses				24
2.11	3-DOF CPVA frequency response left zero point freque	ncy vs.	couple	er	
	stiffness		,	•	25
2.12	2 Frequency response of rotor acceleration over applied va	arying	torque,		
	$\ddot{\alpha}/T$ vs. $\omega$ , for different damping ratios: 0.0, 0.02, 0.05	and 0.1	0		26
	Schematic diagram of CPVA				27
2.14	Effect of mistuning on amplitude of absorber motion vs.	applie	d varyi	_	
	torque level, $r_z$ vs. $\Gamma_{\theta}$		•	•	35
2.15	5 Amplitude of the non-dimensional rotor acceleration vs.	the ap	plied to	orque	
	level, $vv'$ vs. $\Gamma_{\theta}$		•	•	36
2.16	6 Critical torque levels vs. the mistuning level for bifurcat	ion to	non-un	ison	
	and jump, $\Gamma_{\alpha}$ vs. $\varepsilon\sigma$				37
2 12	Rotor system frequency response, non-dimensional roto	r accel	eration		٠.
2.1	applied varying torque, versus varying torque frequency				38
2 1		( 77 / 1	θ 43.7		
	General view of the test facility	، مادنی مک	, 		40
3.2(	a) Test facility partially disassembled, showing main sha absorber attachment point	ut with	Hywne		40
2 20	b) Absorber mass showing bifilar attachment. This is bo	ted to	block s		40
3.2(	in (a)	ileu io	DIOCK S		40
3 3	Experiment system block diagram	•	•		41
	System frequency response with the absorbers locked, $T_0$	-0 25i	Vm		46
	System frequency response when absorbers are free for t				40
7.2	levels: $T_0$ =0.26Nm and 0.53Nm, and mean speed =300RI		iciciii t	_	47
13	System frequency response when absorbers are free with		. level (		
٦.٦	Theory fit from equation (2.26) using 3-DOF CPVA mod	-	10 461 (		, 48
44	System frequency response when absorbers are free for f		ferent i		70
1.7	levels: 0.53Nm, 1.10Nm, 2.20Nm and 4.80Nm	Jui ull		_	49
			•	•	

4.5	System frequency response when absorbers are locked and absorbers are free with 150RPM mean rotor mean and 0.50Nm applied torque.	51
4.6	System frequency response when absorbers are free (cord length is 40.5mm)	
	with torque level 0.50Nm. Theory fit from equation (2.26) using 3-DOF	
	CPVA model	52
4.7	Rotor acceleration vs. applied torque when absorbers are locked .	54
4.8	$ \ddot{\theta} $ vs. $T_{\theta}$ experimental results for locked and unlocked absorbers. The applied	i
	torque frequency is 12.5Hz	55
4.9	$vv'$ vs. $\Gamma_{\theta}$ comparing theoretical and experimental results. The applied torqu	9
	frequency is 12.5Hz	56
4.10	$\left \ddot{ heta} ight $ vs. $T_{ heta}$ showing bifurcation points for different applied torque frequencies	57
4.11	Non-dimensional critical torque level vs. frequency of the applied torque	58
<b>A.1</b>	Linear torsional vibration absorber	62
<b>A.2</b>	System Response of disk 1	63
D.1	System frequency response with various absorbers locked/unlocked. Cord	
	length is $40.5mm$ and torque level is $0.50Nm$	73

#### **CHAPTER 1**

#### Introduction

A multitude of rotating systems suffer from torsional vibration problems that usually arise from some form of fluctuating torques. Typically these torques are periodic with respect to the rotation. Examples are internal combustion engines that receive a torque pulse every time a cylinder fires, or helicopter rotors that have fluctuating loads applied to them as, for example, they pass the fuselage. An efficient way to negate, or at least reduce, the resulting speed fluctuations (vibrations) is through the use of torsional vibration absorbers. In essence, these are additional mass(es) attached to the rotating system and they are constrained to move along a particular path. By carefully designing the geometry, they create a torque that at least partially opposes the applied torque, thus reducing the overall vibration of the system.

Such vibration absorbers have had a long and successful history and a number of theoretical studies have been completed to better understand their behavior. However, surprisingly few systematic experimental studies have been undertaken to substantiate the theoretical predictions. Indeed, practical designs are usually done by a trial and error method and there is no guarantee that an optimum or safe design has been achieved.

In this thesis we focus on designing and executing experiments to investigate the behavior of a centrifugal torsional vibration absorber that moves along a circular path, often called a CPVA (centrifugal pendulum vibration absorber). The results are compared to previously published theoretical results and additional modeling and analysis is completed to explain some of the experiments observed behavior.

The remainder of this chapter presents a brief history of vibration absorber and concludes with an overview of the organization of the thesis.

#### 1.1 History of Vibration Absorbers

Tuned vibration absorbers for vibration and noise suppression were invented almost a century ago. Many designs exist for both the translational type and the torsional type. These range from simple spring mass sub-systems that are added on to a vibrating system to more complicated bi-filar types attached to the crankshaft of IC engines and used to suppress torsional vibration. A literature review of many of the different types of absorbers can be found in the works by Chao and Shaw 1998 and Alsuwaiyan 1999.

Den Hartog 1938 first considered the nonlinear effects in CPVAs and pointed out the shortcomings of circular paths. To resolve the problem, he found a method of mistuning the path so that even for the large amplitudes, the absorbers could work well. However, until about 1980 all practical implementations were based on using circular paths and although some of the nonlinear effects were known, the design of the absorbers was based on linear theory, nonlinear effects being allowed for by a slight over-tuning of the absorber's frequency.

In recent years, there have been many research works on studying varied absorber paths to gain improved performance. Epicycloidal path absorbers have been used in automotive engines (Denman 1992), and Shaw et al. 1998 analyzed other types of paths. In the recent work of Alsuwaiyan 1999, the case of multiple identical absorbers with general paths has been analyzed.

#### 1.2 Objectives and Thesis Organization

The present research has been aimed toward undertaking a systematic experimental study of torsional vibration absorbers and comparing the results to theoretical predictions.

In particular we wish to instrument the experimental facility, calibrate the instrumentation and record the system response due to applied harmonically oscillating torque input. The system run at constant mean speeds and various forcing frequencies, torque levels, and absorber tunings. Only two absorbers were attached and they were constrained to move along circular paths.

The remainder of the thesis is organized as follows. Chapter 2 presents a review of some of the related theory. Much of this is a repetition of work that can be found elsewhere, but is included here both by way of an introduction to the ideas of absorbers, and also to make the comparison between theoretical and experimental results easier to accomplish. Moreover, some additional modeling of the system to allow for experimentally observed behavior is included in Section 2.2.2. The final section of Chapter 2 includes a number of different theoretical response plots to give one an appreciation of how the system might be expected to behave in the nonlinear regime.

Chapter 3 and 4 deal with the experimental aspects of the work. Chapter 3 discusses the experimental set-up while Chapter 4 deals more with the actual presentation of the results and their comparison with the theoretical predictions.

The final Chapter discusses some of the findings and lists recommendations for future work.

#### **CHAPTER 2**

### **Theoretical Review and Numerical Examples**

In this chapter, we review some of the theory behind vibration absorbers. By way of an introduction to the general CPVA problem, the standard translational spring-mass absorber is first introduced. Next, linear analysis of the 2-DOF and 3-DOF pendulum vibration absorber is presented. The final section outlines theory presented in Alsuwaiyan, (1999) that deals with the more general case of a CPVA where the path is not restricted to a circle and nonlinearitites are included. It is included here as the results will be used to compare with the experimental results of Chapter 4.

#### 2.1 Spring-Mass Absorber

Consider the 2 DOF system shown in Figure 2.1. Adopting the notation used by Den Hartog 1956, and following his development, the equations of motion for the system are:

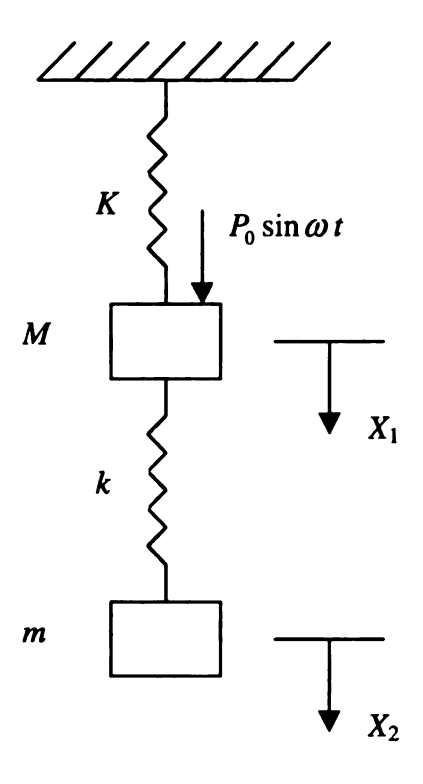


Figure 2.1 Spring-mass absorber

$$M\ddot{X}_{1} + (K+k)X_{1} - kX_{2} = P_{0} \sin \omega t$$

$$m\ddot{X}_{2} + k(X_{2} - X_{1}) = 0$$
(2.1)

Introducing the following terms:

$$X_{st} = P_0 / K$$

$$\omega_a^2 = k / m$$

$$\Omega_n^2 = K / M$$

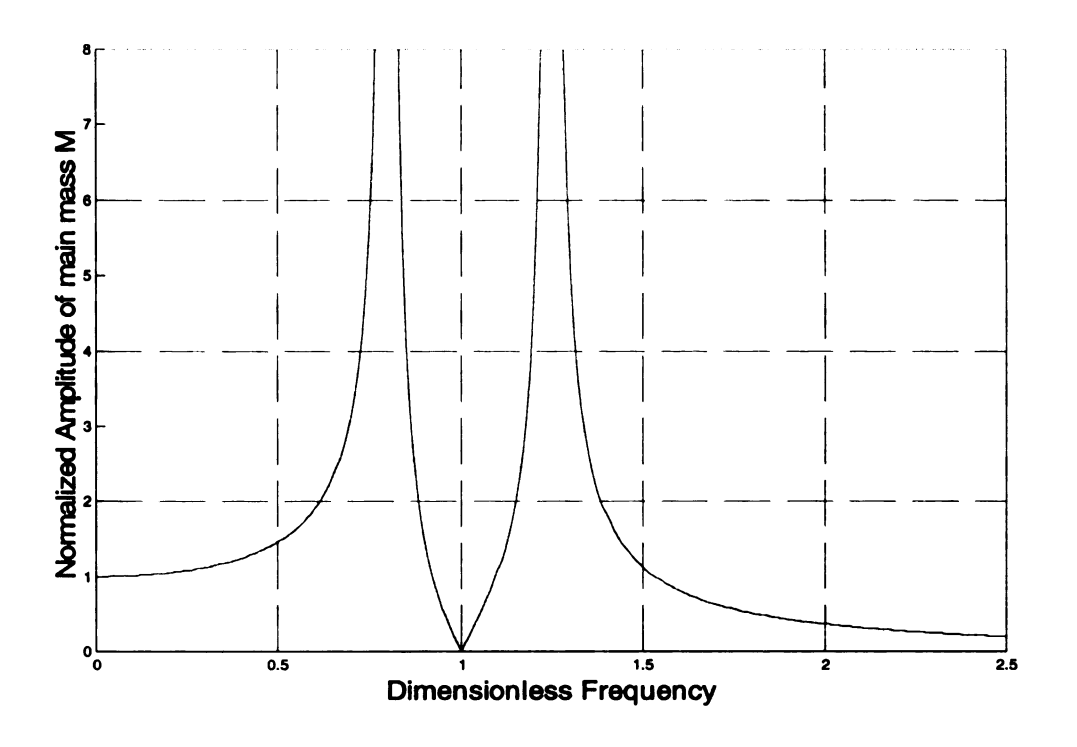
$$\mu = m / M$$
(2.2)

and solving equation (2.1), the normalized amplitude  $a_1/X_{st}$  of the main mass M and the normalized amplitude  $a_2/X_{st}$  of the absorber mass m are:

$$\frac{a_{1}}{X_{st}} = \frac{1 - \frac{\omega^{2}}{\omega_{a}^{2}}}{\left(1 - \frac{\omega^{2}}{\omega_{a}^{2}}\right)\left(1 + \frac{k}{K} - \frac{\omega^{2}}{\Omega_{n}^{2}}\right) - \frac{k}{K}} \\
\frac{a_{2}}{X_{st}} = \frac{1}{\left(1 - \frac{\omega^{2}}{\omega_{a}^{2}}\right)\left(1 + \frac{k}{K} - \frac{\omega^{2}}{\Omega_{n}^{2}}\right) - \frac{k}{K}} \tag{2.3}$$

The system response vs. frequency is shown in Figure 2.2 for  $\mu$ =1/5 and  $\omega_a$ = $\Omega_n$ . As would be expected, the addition of the second (absorber) mass adds another resonance to the system. However, the motion of the main mass, M, can now be reduced to zero when the absorber frequency,  $\omega_a$ , equals the driving frequency,  $\omega$ . At this particular frequency the motion of the absorber generates an equal but opposite force to the applied force, thus bringing the main mass to rest. While this can be of considerable benefit, and indeed is the main reason for the addition of an absorber, if the forcing frequency should change from the value of  $\omega_a$  large resonant responses can result. The addition of damping will alleviate this at the expense of raising the minimum point to a nonzero value. Damping will also broaden the effective frequency range of the absorber but it still suffers from the fact that if the forcing frequency changes a great deal, the absorber will applify the motion instead of reducing it. The natural question is, can an absorber be

designed that will remain "tuned" if the forcing frequency changes? In general this is difficult if not impossible to achieve, but for applications involving rotating systems such absorbers can be designed. These are introduced in the next section.



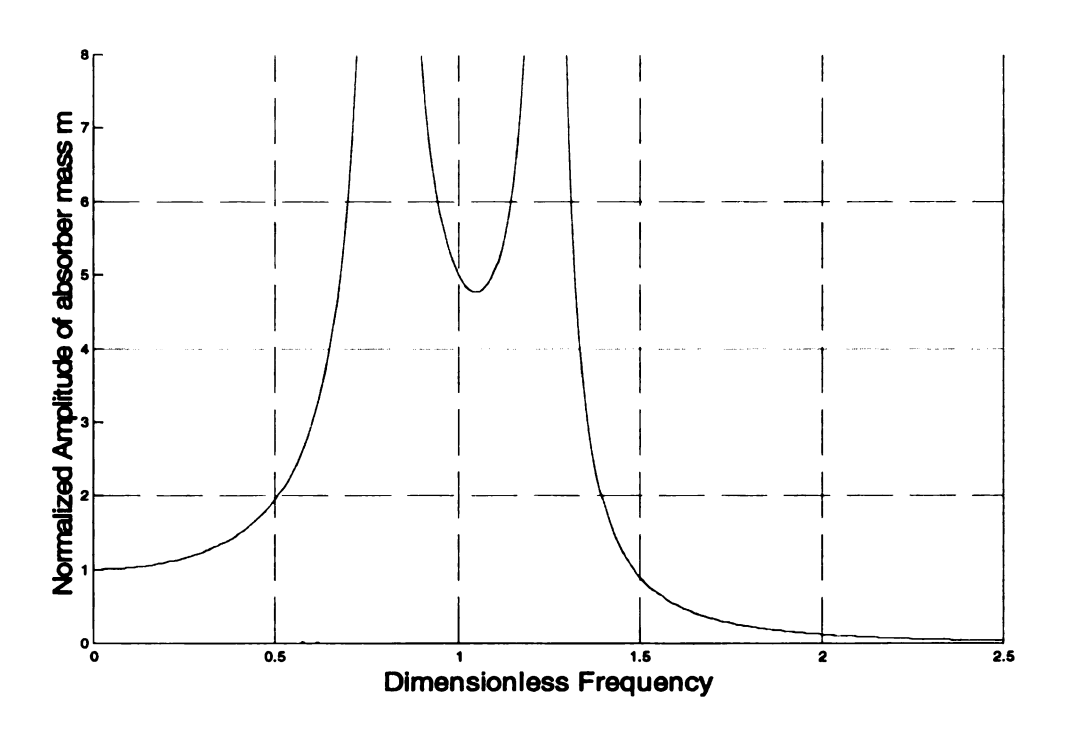


Figure 2.2 Normalized amplitude of the main mass and that of the absorber mass vs. dimensionless frequency,  $\omega/\omega_a$ 

#### 2.2 Torsional Vibration Absorber

#### 2.2.1 Modeling of a Centrifugal Pendulum Vibration Absorber (CPVA)

Unlike the translational absorber just discussed, often the forcing frequency applied to the system is not a constant. Rotational systems are a case where very often the frequency of the disturbance is at, or a multiple of, the speed of rotation. Examples of this type of problem can be found in works by Taylor 1936 and Den Hartog 1938. The essential difference between centrifugal torsional vibration absorbers and their translational counterparts is that the restoring force of the absorber is generated from the centrifugal field and is thus proportional to the square of the rotational speed. That is, it changes with the operating speed of the system. This is exactly the result that is needed for the absorber to remain "tuned" at all operating speeds. The details of this will now be presented.

Figure 2.3 shows the essential components of a centrifugal pendulum vibration absorber. This is a 2-DOF nonlinear system where  $\theta$  describes the angular displacement of the flywheel and  $\phi$  is the relative angular displacement of the absorber. J is the moment of inertia of the flywheel and m is the mass of the absorber, which is taken as a point mass. T(t) is the applied torque.

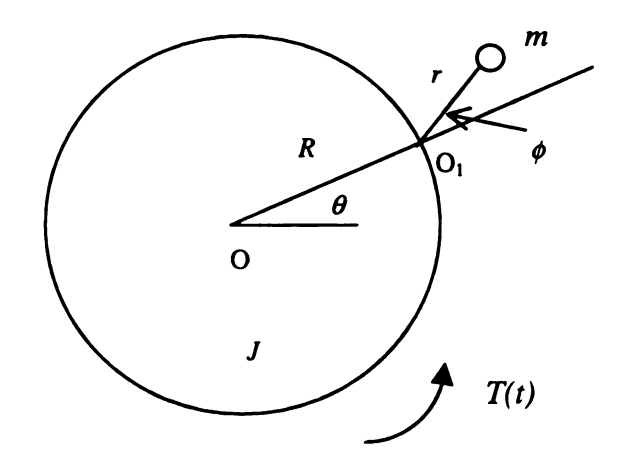


Figure 2.3 Centrifugal Pendulum Vibration Absorber

We use Newton's Law to derive the motion equations for this 2-DOF vibrating system. The free body diagram is shown in Figure 2.4.

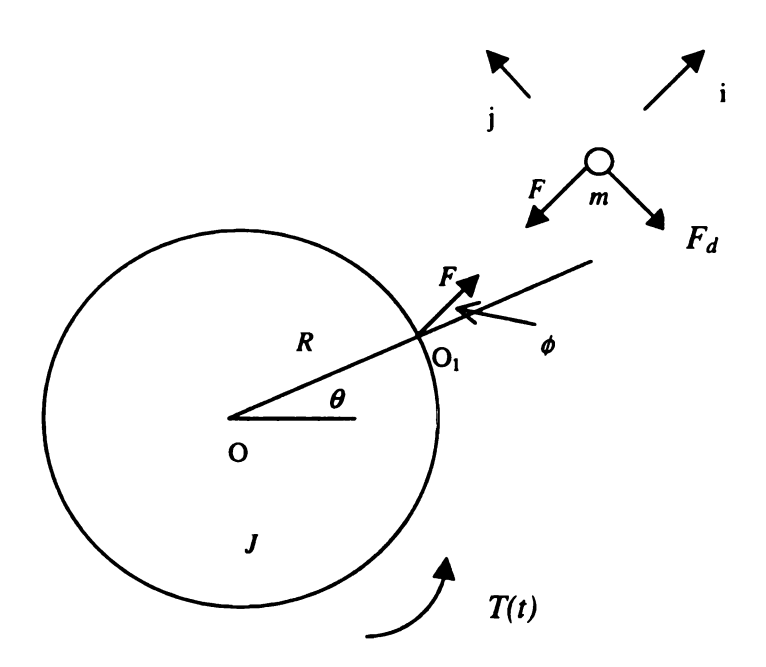


Figure 2.4 Free body diagram of CPVA

F is the tension force along the pendulum absorber cord and  $F_d$  is the damping force imposed on the pendulum absorber, which is modeled as:

$$F_d = cr\dot{\phi} \tag{2.4}$$

Noting that the absolute acceleration of the mass m is:

$$\vec{a}_{m} = \left\{ R\ddot{\theta}\sin\phi - R\dot{\theta}^{2}\cos\phi - r(\dot{\theta} + \dot{\phi})^{2}\right\} \vec{i} + \left\{ R\ddot{\theta}\cos\phi + R\dot{\theta}^{2}\sin\phi + r(\ddot{\theta} + \ddot{\phi})\right\} \vec{j}$$
(2.5)

The absorber's equation of motion in the i-direction is:

$$F = m \left\{ -R\ddot{\theta}\sin\phi + R\dot{\theta}^2\cos\phi + r(\dot{\theta} + \dot{\phi})^2 \right\}$$
 (2.6)

and in the j-direction it is:

$$cr\dot{\phi} = -m\left\{R\ddot{\theta}\cos\phi + R\dot{\theta}^2\sin\phi + r(\ddot{\theta} + \ddot{\phi})\right\} \tag{2.7}$$

The equation of motion for the flywheel is:

$$J\ddot{\theta} = T(t) + FR\sin\phi \tag{2.8}$$

using equation (2.6) to substitute for the unknown force, F, equations (2.7 and 2.8) then define the nonlinear equations of motion for the CPVA system. Rearranging, they are:

$$J\ddot{\theta} + m \left\{ R\ddot{\theta} \sin \phi - R\dot{\theta}^{2} \cos \phi - r(\dot{\theta} + \dot{\phi})^{2} \right\} R \sin \phi = T(t)$$

$$R\ddot{\theta} \cos \phi + R\dot{\theta}^{2} \sin \phi + r(\ddot{\theta} + \ddot{\phi}) + \frac{cr}{m} \dot{\phi} = 0$$
(2.9)

These can be further simplified if we restrict the motion of the absorber to be small  $(\phi << 1)$  and if we assume the applied torque to be  $T\sin(\omega t)$  and the motion of the wheel to be a steady rotation speed  $\Omega$  plus a small sinusoidal oscillation of frequency  $\omega$  with the phase angle  $\gamma$ .

$$\theta(t) = \Omega t + \beta(t)$$
  

$$\beta(t) = \theta_0 \sin(\omega t + \gamma)$$
(2.10)

Linearizing equation (2.9), we can get:

$$J \ddot{\beta} - mR(R+r)\Omega^{2}\phi = T \sin \omega t$$

$$(R+r)\ddot{\beta} + r\ddot{\phi} + \frac{c}{m}r\dot{\phi} + R\Omega^{2}\phi = 0$$
(2.11)

defining the following vectors:

$$\vec{X} = \begin{pmatrix} \beta \\ \phi \end{pmatrix} = \begin{pmatrix} \theta_0 \\ \phi_0 \end{pmatrix} e^{i\alpha x}, \quad \vec{T} = \begin{pmatrix} T \\ 0 \end{pmatrix}$$
 (2.12)

equation (2.11) can be written in the following complex matrix form:

$$\begin{bmatrix} J & 0 \\ R+r & r \end{bmatrix} \ddot{\vec{X}} + \begin{bmatrix} 0 & 0 \\ 0 & \frac{c}{m}r \end{bmatrix} \dot{\vec{X}} + \begin{bmatrix} 0 & -mR(R+r)\Omega^2 \\ 0 & R\Omega^2 \end{bmatrix} \vec{X} = \vec{T}e^{i\omega t}$$
 (2.13)

or, using the standard notation:

$$M\ddot{\vec{X}} + C\dot{\vec{X}} + K\vec{X} = \vec{T}e^{i\omega t}$$
 (2.14)

Considering only steady-state solutions

$$\vec{X} = \left(-\omega^2 M + i\omega C + K\right)^{-1} \vec{T} e^{i\omega t} \tag{2.15}$$

i.e.,

$$\vec{X} = \begin{bmatrix} -\omega^2 J & -mR(R+r)\Omega^2 \\ -\omega^2(R+r) & (R\Omega^2 - r\omega^2) + i\left(\frac{c}{m}r\omega\right) \end{bmatrix}^{-1} \vec{T}e^{i\omega\tau}$$
 (2.16)

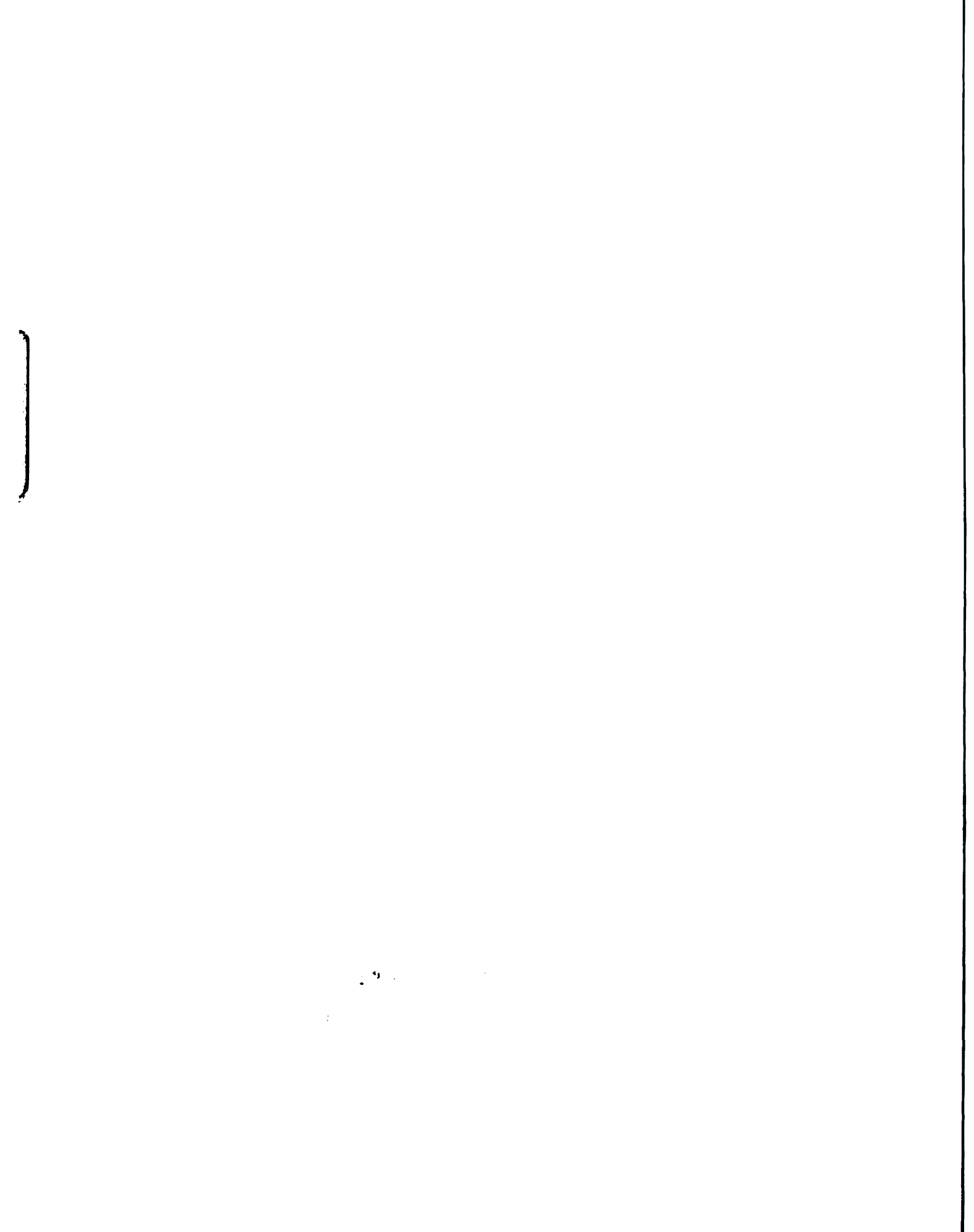
We will now consider the undamped and the damped case separately,

#### 2.2.1.1 The Undamped Absorber

When the damping is zero, c=0, the amplitude of the steady-state solutions,  $\theta_0$  and  $\phi_0$ , can be written as:

$$\theta_0 = \frac{(r\omega^2 - R\Omega^2)/\omega^2}{J(R\Omega^2 - r\omega^2) + mR(R+r)^2\Omega^2} T$$

$$\phi_0 = \frac{-(R+r)}{J(R\Omega^2 - r\omega^2) + mR(R+r)^2\Omega^2} T$$
(2.17)



Recalling that  $\theta_0$  is the amplitude of motion of the flywheel due to the applied fluctuating torque, we can clearly see that  $\theta_0$  is zero if

$$\omega = \Omega \sqrt{\frac{R}{r}} \tag{2.18}$$

As was previously mentioned, the frequency of the applied torque,  $\omega$ , is likely to be proportional to the rotating speed,  $\Omega$ . Calling this constant of proportionality,  $\tilde{n}$ , we therefore have  $\omega = \tilde{n}\Omega$  and so for  $\theta_0$  to be zero, we require,

$$\tilde{n}^2 = \frac{R}{r} \tag{2.19}$$

i.e. the absorber can be "tuned" to absorb a certain vibration of order  $\tilde{n}$ . Figure 2.5 graphically shows this by plotting the response of the system as a function of  $\omega$ . The system parameters for this plot are set at:  $\tilde{n}=2$ , R=1.00m, r=0.25m,  $\Omega=\pi rad/s$ , m=1.00kg, J=20.0Kg  $m^2$ . The main points to note here are that when  $\omega=\tilde{n}$   $\Omega=2\pi rad/s=1$ Hz, the amplitude  $\theta_0$  is identically zero. However, a non-rigid body resonance occurs at  $\omega=\sqrt{1+\frac{m(R+r)^2}{J}}\tilde{n}\Omega=1.04$ Hz.

An alternative way of plotting these results is to use the acceleration values of the flywheel and the absorber. For completeness, these are plotted in Figure 2.6. Using this ordinate it is easier to appreciate the meaning of the rigid body resonance that occurs at  $\omega=0$ . The value of  $\ddot{\theta}/T \to 1/(J+m(R+r)^2)$  as  $\omega \to 0$ , i.e., for the parameter value chosen here this limit is 0.0449.



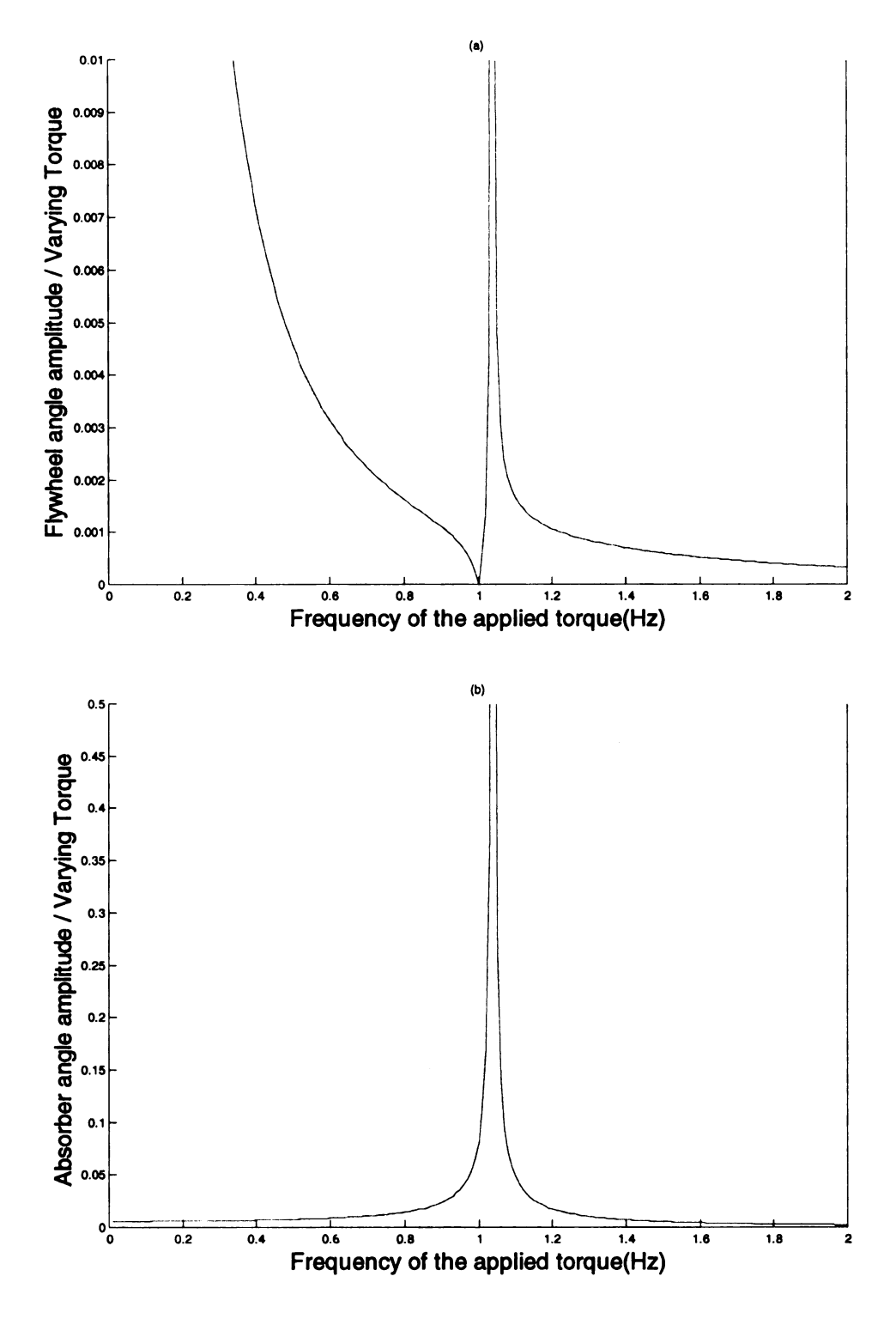


Figure 2.5 Undamped CPVA frequency response plots (a) $\theta_0/T$  vs.  $\omega$  and (b) $\phi_0/T$  vs.  $\omega$ 



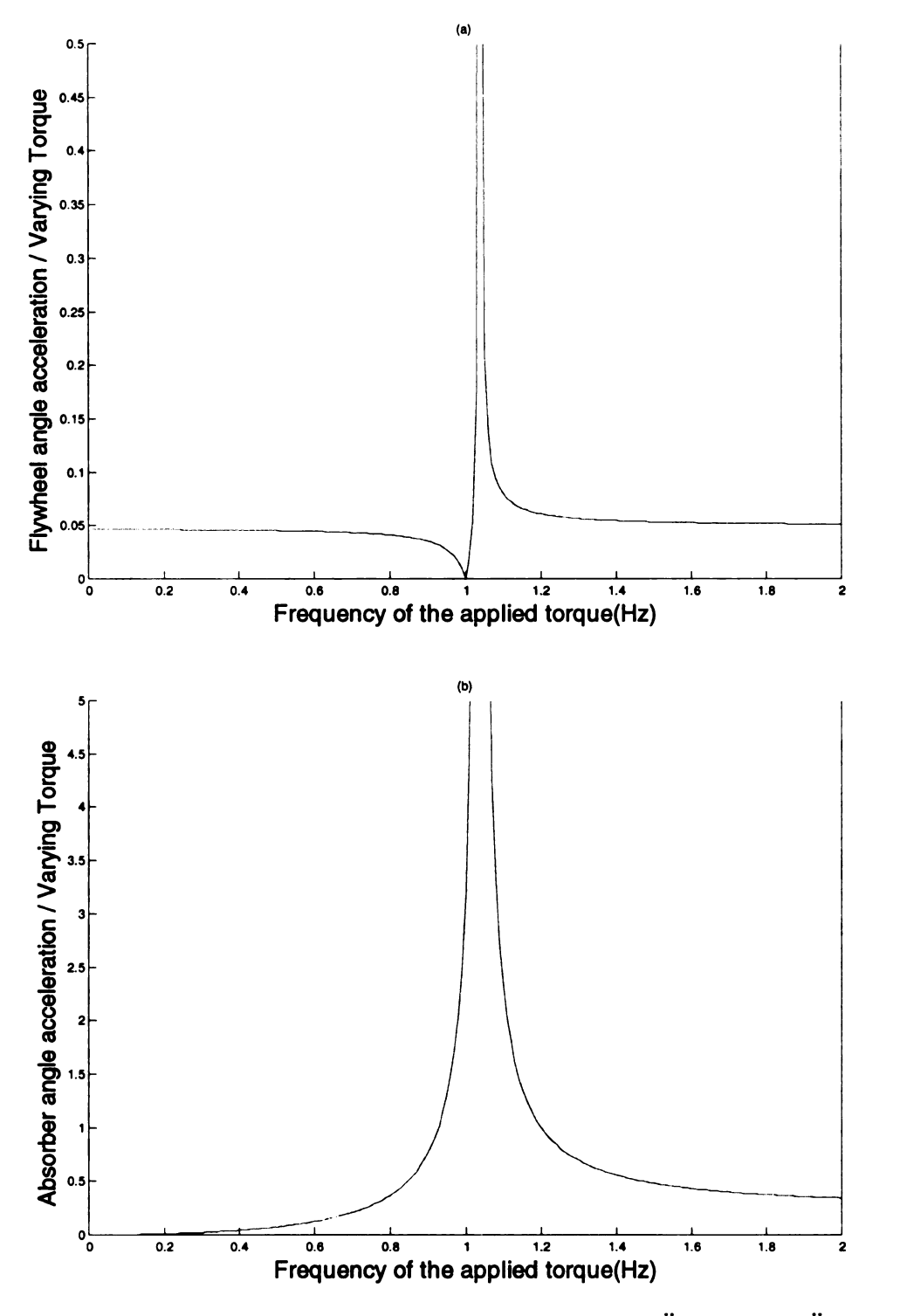


Figure 2.6 Undamped CPVA frequency response plots (a)  $\ddot{\theta}$  /T vs.  $\omega$  (b)  $\ddot{\phi}$  /T vs.  $\omega$ 

#### 2.2.1.2 The Damped Absorber

The steady-state solutions for the damped case can be found analytically by solving the matrix inverse problem of equation (2.16). Rather than doing this, specific solutions are calculated for the same set of parameters used in the previous subsection, i.e,  $\tilde{n} = 2$ , R=1.00m, r=0.25m,  $\Omega = \pi rad/s$ , m=1.00kg, J=20.0Kg  $m^2$ . In addition, we wish to study the influence of the damping c. Following the usual practice, we define a damping ratio,  $\xi$ , such that equation (2.11) yields repeated eigenvalues of -1 when  $\xi = 1$ , i.e.

$$\xi = \frac{c}{2m\tilde{n}\Omega} \tag{2.20}$$

The results are plotted in Figure 2.7 for damping ratios of 0.0, 0.02, 0.05 and 0.10. We can observe that as the damping ratio is increased, the frequency response minimum point moves slightly to the left. Moreover, for non-zero damping it is no longer possible for the absorber to totally cancel the oscillation of the flywheel.

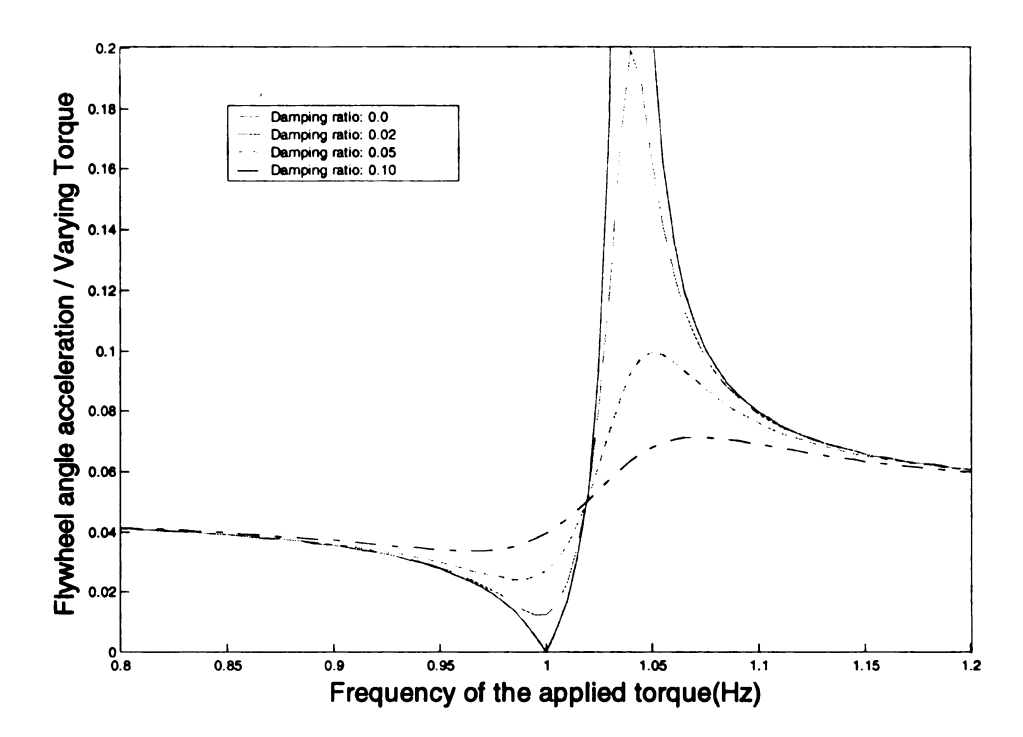


Figure 2.7 Frequency response of flywheel acceleration,  $\ddot{\theta}$  /T vs.  $\omega$ , for different damping ratio: 0.0, 0.02, 0.05 and 0.10

#### 2.2.2 3-Degree Of Freedom CPVA

In the experimental results, which will be presented in Chapter 4, it was found that the system did not respond exactly as the 2 DOF model just discussed. It seemed as if there was some torsional compliance between the motor drive shaft and the flywheel that the absorbers were attached to. To gain some insight into this, an additional degree-of-freedom was added to allow for the shaft's stiffness. The 3-DOF system is sketched in Figure 2.8. As before, the radius of the flywheel is called R, and the distance between the absorber mass central gravity and the edge of the flywheel is r. A damping coefficient, c, is added as before. The moment of inertias of the motor drive (from now on, we shall call this the rotor) and flywheel are  $I_1$  and  $I_2$  respectively. K is the stiffness of the coupler between the rotor and the flywheel. The rotor has a varying torque T sin ot applied to it.

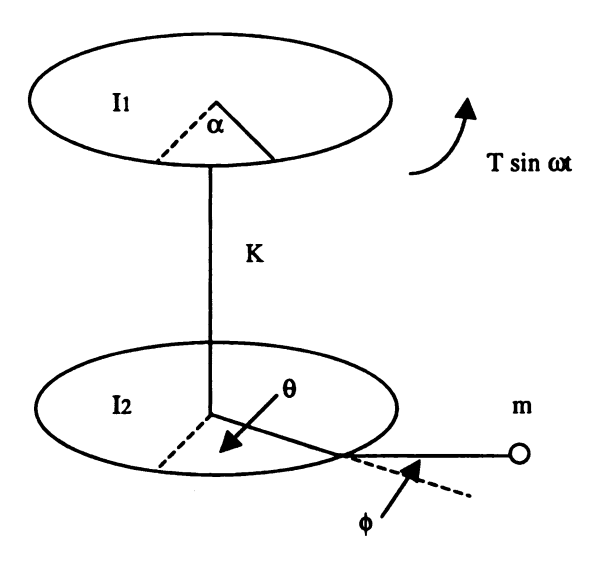


Figure 2.8 3-DOF CPVA

Using Newton's method, the linear equations of motion for this system can be written as:

$$I_{1}\ddot{\alpha} + K(\alpha - \theta) = T \sin \omega t$$

$$I_{2}\ddot{\theta} - mR(R + r)\Omega^{2}\phi + K(\theta - \alpha) = 0$$

$$(R + r)\ddot{\theta} + r\ddot{\phi} + \frac{c}{m}r\dot{\phi} + R\Omega^{2}\phi = 0$$

$$(2.21)$$

where  $\Omega$  is the mean speed of the rotor.

Defining the following vectors:

$$\vec{X} = \begin{pmatrix} \alpha \\ \theta \\ \phi \end{pmatrix} \quad \vec{T} = \begin{pmatrix} T \\ 0 \\ 0 \end{pmatrix} \tag{2.22}$$

equation (2.21) can be written in complex matrix form as

$$\begin{bmatrix} I_1 & 0 & 0 \\ 0 & I_2 & 0 \\ 0 & R+r & r \end{bmatrix} \ddot{\vec{X}} + \begin{bmatrix} 0 & 0 & 0 \\ 0 & 0 & 0 \\ 0 & 0 & \frac{c}{m} r \end{bmatrix} \dot{\vec{X}} + \begin{bmatrix} K & -K & 0 \\ -K & K & -mR(R+r)\Omega^2 \\ 0 & 0 & R\Omega^2 \end{bmatrix} \vec{X} = \vec{T}e^{i\omega t} \quad (2.23)$$

or, in the usual notation,

$$M\ddot{\vec{X}} + C\dot{\vec{X}} + K\vec{X} = \vec{T}e^{i\omega\tau}$$
 (2.24)

Considering only steady-state solutions, we have:

$$\vec{X} = (-\omega^2 M + i\omega C + K)^{-1} \vec{T} e^{i\omega t}$$
(2.25)

or in more detail

$$\bar{X} = \begin{bmatrix}
-\omega^2 I_1 + K & -K & 0 \\
-K & -\omega^2 I_2 + K & -mR(R+r)\Omega^2 \\
0 & -\omega^2 (R+r) & (R\Omega^2 - r\omega^2) + i\left(\frac{c}{m}r\omega\right)
\end{bmatrix}^{-1} \bar{T}e^{i\omega t} \tag{2.26}$$

We now analysis this solution for both the undamped and damped absorber.

#### 2.2.2.1 The Undamped Absorber

For this 3-DOF system, when the absorber is locked, the flywheel itself functions as a vibration absorber for the rotor (details are given in Appendix A). Hence, if the absorbers are free to move, two minimum points (absorber frequencies) occur. To demonstrate this, Figure 2.9 shows the frequency response of the rotor acceleration normalized by the applied varying torque. The system parameters are:  $\tilde{n} = 2$ , R = 1.00m, r = 0.25m,  $\Omega = \pi rad/s$ , m = 1.00kg,  $I_1 = 1.00kgm^2$ ,  $I_2 = 20.00kgm^2$ , K = 10000Nm/rad. The two minimum points in the frequency response are close to 1.0Hz, the CPVA's own natural frequency ( $\frac{\Omega}{2\pi}\sqrt{\frac{R}{r}}$ ), and

close to 3.6Hz, which is approximately the natural frequency of the flywheel,

$$\frac{1}{2\pi}\sqrt{\frac{K}{I_2}}.$$

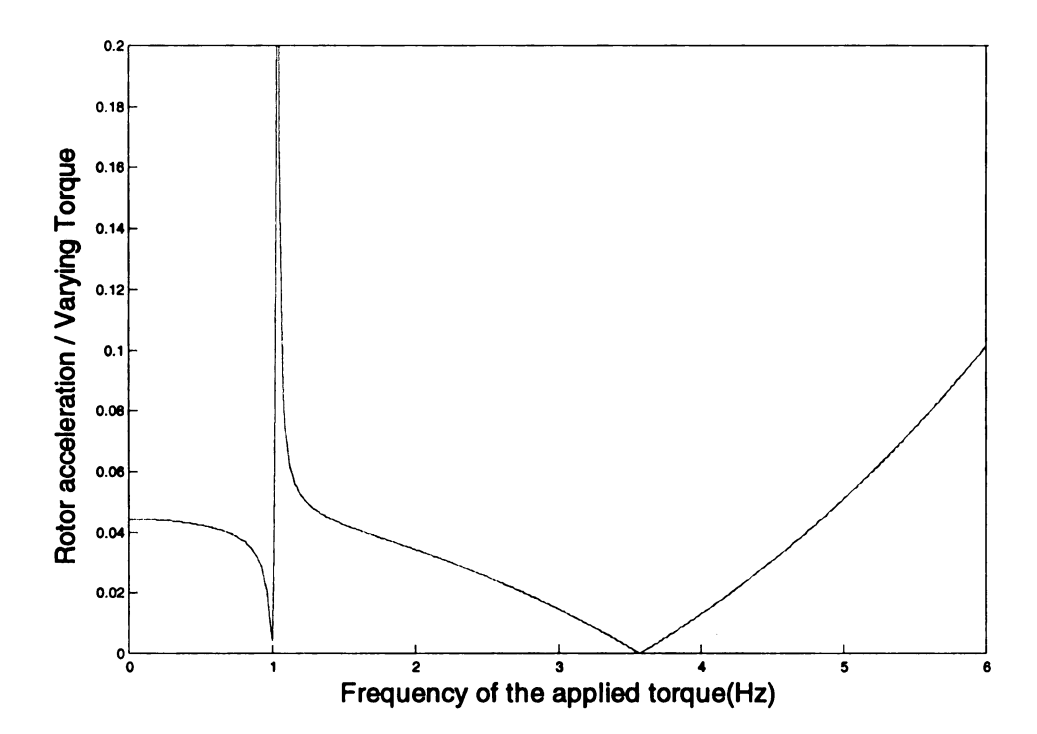


Figure 2.9 Frequency response of rotor acceleration over applied varying torque,  $\ddot{\alpha}/T$  vs.  $\omega$ 

However, the first minimum point is also a function of the coupler stiffness, K. It only tends to  $\frac{\Omega}{2\pi}\sqrt{\frac{R}{r}}$  as K tends to infinity (i.e. the 2 DOF case). Figure 2.10 shows the rotor acceleration versus  $\omega$  for different coupler stiffnesses. The minimum point moves to the left with decreasing coupler stiffness.

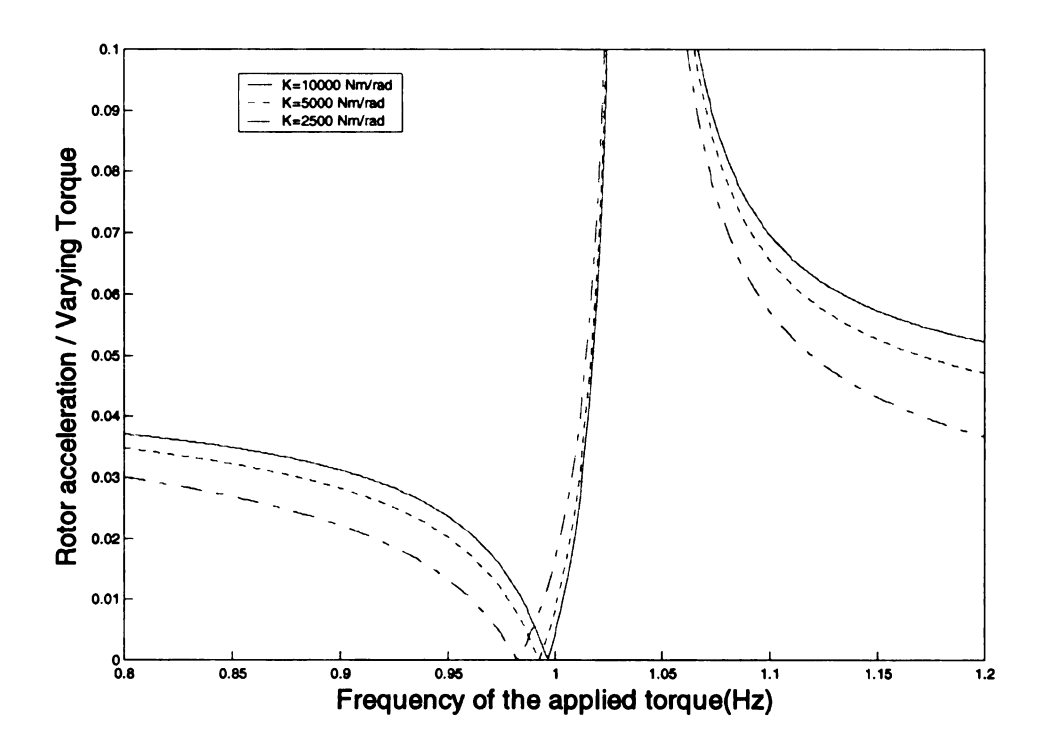


Figure 2.10 Frequency response of rotor acceleration over applied varying torque,  $\ddot{\alpha}/T$  vs.  $\omega$ , for different coupler stiffnesses

To study this trend analytically, we can use equation (2.26) to find the zero points. They occur at values of  $\omega$  that satisfy:

$$m\omega^{2}(R+r)^{2}R\Omega^{2} = (k-\omega^{2}I_{2})(R\Omega^{2}-r\omega^{2})$$
 (2.27)

Figure 2.11 shows the solution of equation (2.27) for the left zero point as a function of the coupler stiffness. The other parameters are the same as used to create Figure 2.9.

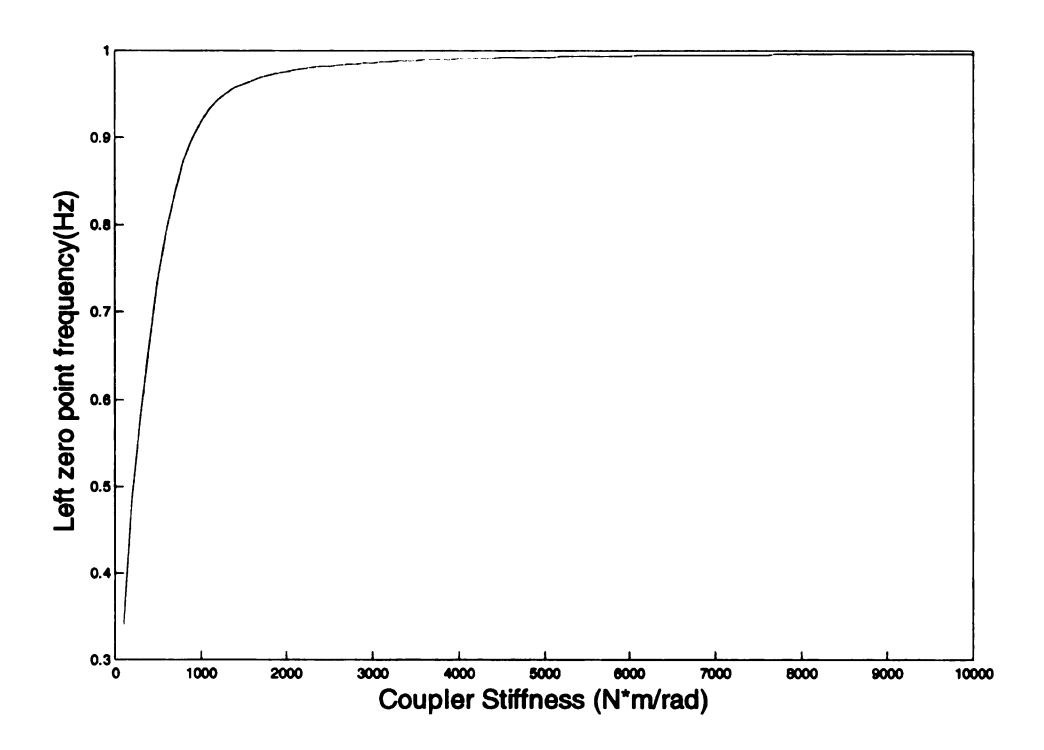


Figure 2.11 3-DOF CPVA frequency response left zero point frequency vs. coupler stiffness

## 2.2.2.2 The Damped Absorber

Using the damping ratio as defined by equation (2.20) and the same parameter values as in Figure 2.9, Figure 2.12 shows the influence of varying the damping ratio from 0.0 to 0.1. As for the 2 DOF case, the minimum point moves to the left with increasing damping ratio. Also, the rotor acceleration can not be reduced to zero when the absorber has damping.

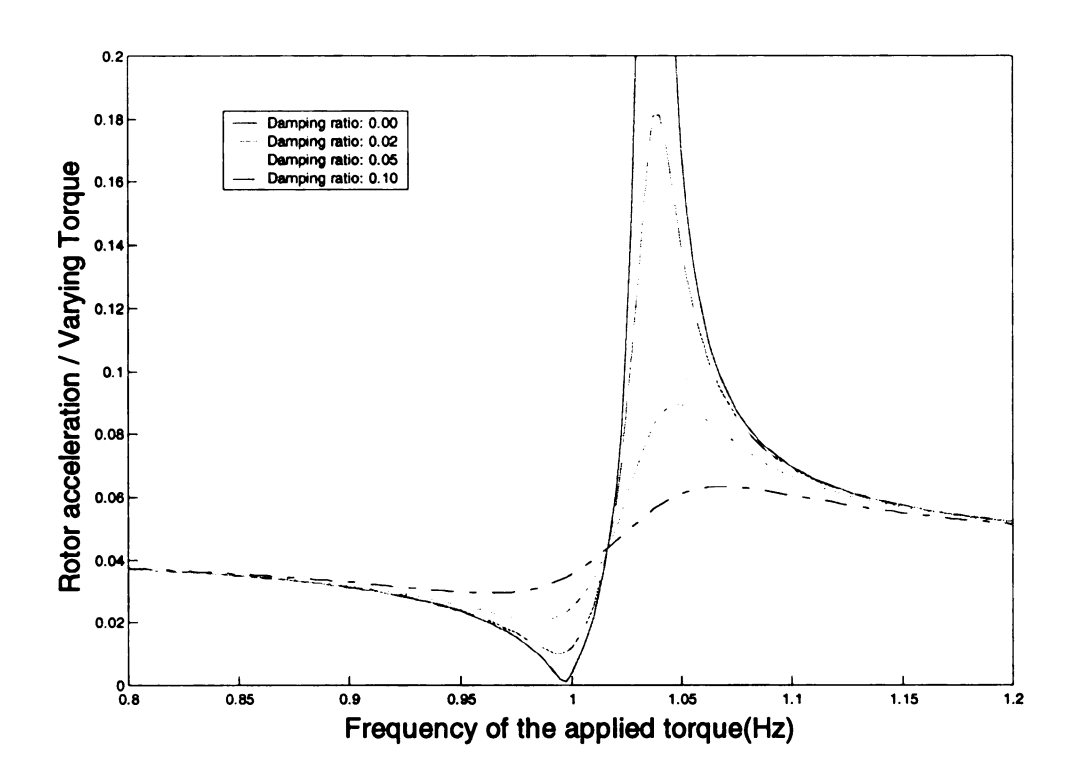


Figure 2.12 Frequency response of rotor acceleration over applied varying torque,  $\ddot{\alpha}/T$  vs.  $\omega$ , for different damping ratios: 0.0, 0.02, 0.05 and 0.10

### 2.2.3 Equations for a CPVA Moving Along a General Path

The proceeding sections in this chapter have presented somewhat simplified models of real systems. No solutions have been sought that allow for nonlinear effects. In this section such effects are accounted for and approximate solutions found. It is a summary of past work by Alsuwaiyan (1999) and is included here for completeness. The presentation will also aid in the important task of relating the theoretical work to the experimental results and enable us to clearly define the notation.

The system consists of a uniform wheel of inertia, J, that rotates about its center, O, as shown in Figure 2.13. There are N CPVAs attached to the wheel (only the i<sup>th</sup> one is shown in the figure) and they move along symmetric paths.  $R_i$  is the distance from the i<sup>th</sup> absorber central gravity to the center of rotation and  $S_i$  is the arc length of i<sup>th</sup> absorber path. At each vertex of the i<sup>th</sup> absorber path, this distance is  $R_{i0}$ , i.e.,  $R_i(S_i=0)=R_{i0}$ .  $\theta$  is the angular orientation of the disk relative to an inertial frame of the reference and  $m_i$  is the mass of the i<sup>th</sup> absorber.

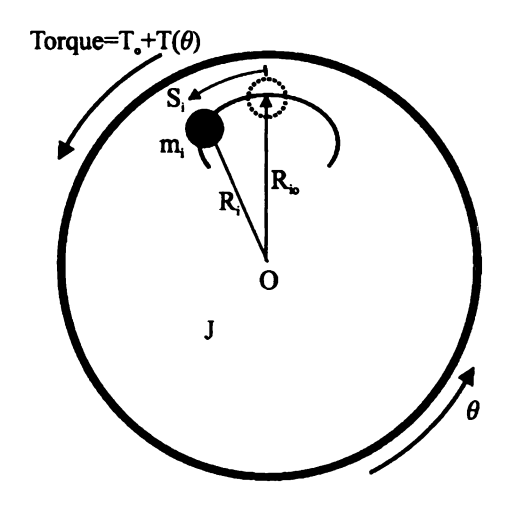


Figure 2.13 Schematic diagram of CPVA

Using Lagrange's method to derive the equations of motion, we first need to find the total kinetic energy of the system. The kinetic energy of wheel is given by:

$$T_r = \frac{1}{2}J\dot{\theta}^2$$

The kinetic energy of the ith absorber is:

$$T_{ai} = \frac{1}{2} m_i \vec{v}_i \cdot \vec{v}_i$$

where the  $\vec{v}_i$  is the velocity of the i<sup>th</sup> absorber, which is

$$\vec{v}_i = R_i \dot{\theta} \; \vec{e}_{\theta} + \dot{S}_i \; \vec{e}_{s_i}$$

where  $\vec{e}_{\theta}$  and  $\vec{e}_{S_i}$  are unit vectors in the  $\theta$  and Si direction respectively. By geometry, the following relationship holds:

$$(dS_i)^2 = (dR_i)^2 + (R_i d\phi_i)^2$$

and so we have:

$$\frac{d\phi_i}{dS_i} = \frac{1}{R_i} \sqrt{1 - \left(\frac{dR_i}{dS_i}\right)^2}$$

$$\vec{e}_{\theta} \bullet \vec{e}_{S_i} = \sqrt{1 - \left(\frac{dR_i}{dS_i}\right)^2}$$

Hence, the total kinetic energy of the system is given by:

$$T = \frac{1}{2} \left( J\dot{\theta}^{2} + \sum_{i=1}^{N} m_{i} \left( X_{i}\dot{\theta}^{2} + \dot{S}_{i}^{2} + 2\dot{\theta}\dot{S}_{i}\tilde{G}_{i} \right) \right)$$

where

$$X_{i}(S_{i}) = R_{i}^{2}(S_{i})$$

$$\tilde{G}_{i}(S_{i}) = \sqrt{X_{i}(S_{i}) - \frac{1}{4} \left(\frac{dX_{i}}{dS_{i}}(S_{i})\right)^{2}}$$

$$(2.28)$$

The only source of potential energy for this system is gravitational, and this is assumed to be small compared to the kinetic energy. We can now proceed to apply Langrange's equations. In the usual notation

$$\frac{d}{dt} \left( \frac{\partial T}{\partial \dot{q}_l} \right) - \frac{\partial T}{\partial q_l} = Q_l, \quad l = 1, ..., N + 1$$

where  $q_1=0$ , and  $q_j=S_i$ , j=2,3,...,N+1, and i=1,2,...,N are the generalized coordinates and the  $Q_i$ 's are the generalized forces, which arise from damping and applied torque, and are given by,

$$Q_{1} = -c_{0}\dot{\theta} + \sum_{i=1}^{N} c_{ai}\dot{S}_{i}\tilde{G}_{i} + T_{0} + T(\theta)$$

$$Q_{i} = -c_{ai}\dot{S}_{i}, \quad j = 2,3,...,N+1$$

where  $c_{ai}$  and  $c_0$  are the damping coefficients for the  $i^{th}$  absorber and the rotor, respectively. Applying Langrange's equations, the equations of motion for the system can be written as:

$$m_i \left( \ddot{S}_i + \tilde{G}_i(S_i) \ddot{\theta} - \frac{1}{2} \frac{dX_i}{dS_i} (S_i) \dot{\theta}^2 \right) = -c_{ai} \dot{S}_i$$
 (2.29)

$$J\ddot{\theta} + \sum_{i=1}^{N} m_i \left( \frac{dX_i}{dS_i} (S_i) \dot{S}_i \dot{\theta} + X_i (S_i) \ddot{\theta} + \tilde{G}_i (S_i) \ddot{S}_i + \frac{d\tilde{G}_i}{dS_i} (S_i) \dot{S}_i^2 \right)$$

$$= \sum_{i=1}^{N} (c_{ai} \tilde{G}_i (S_i) \dot{S}_i) - c_0 \dot{\theta} + T_0 + T(\theta)$$
(2.30)

These can be further simplified and made amenable to analysis by assuming that all absorbers have equal masses,  $m_i=m$ , and equal damping,  $c_{ai}=c_a$ , and all paths have the same value of  $R_i$  at each vertex,  $R_{i0}=R_0$ .

By introducing the following terms:

$$s_i = S_i / R_{i0}, \ \tilde{g}_i(s_i) = \tilde{G}_i(S_i) / R_{i0}, \ b_i = I_i / J,$$
  
 $I_i = m_i R_{i0}^2, \ \mu_{ai} = c_{ai} / m_i \Omega, \ \mu_0 = c_0 / J \Omega,$   
 $\Gamma_0 = T_0 / J \Omega^2, \ \Gamma(\theta) = T(\theta) / J \Omega^2$ 

and

$$\begin{aligned}
x_i(s_i) &= X_i / R_{i0}^2, \\
\tilde{g}_i(s_i) &= \sqrt{x_i(s_i) - \frac{1}{4} \left(\frac{dx_i}{ds_i}(s_i)\right)^2}
\end{aligned}$$

and

$$b_0 = \frac{I_0}{J}, I_0 = m_0 R_0^2, \mu_a = \frac{Nc_a}{m_0 \Omega}, m_0 = Nm$$

Moreover, a new nondimensional variable  $v = \frac{\dot{\theta}}{\Omega}$  has been introduced where  $\Omega$  is the mean speed of the wheel. The notation (.)' means differentiation with respect to the rotor angular,  $\theta$ .

After equation (2.30) are nondimensionalized, and the independent variable is changed from t to  $\theta$ , the equations of motion become

$$vs_{i}'' + [s_{i}' + \tilde{g}_{i}(s_{i})]v' - \frac{1}{2}\frac{dx_{i}}{ds_{i}}(s_{i})v = -\mu_{ai}s_{i}'$$

$$vv' + \frac{b_{0}}{N}i\sum_{i=1}^{N} \left(\frac{dx_{i}}{ds_{i}}s_{i}'v^{2} + x_{i}(s_{i})vv' + \tilde{g}_{i}(s_{i})s_{i}'vv' + \tilde{g}_{i}(s_{i})s_{i}'v^{2} + \frac{d\tilde{g}_{i}}{ds_{i}}(s_{i})s_{i}^{2}v^{2}\right)$$

$$= \frac{b_{0}}{N}\sum_{i=1}^{N} \mu_{a}\tilde{g}_{i}(s_{i})s_{i}'v - \mu_{0}v + \Gamma_{0} + \Gamma(\theta)$$
(2.31)

It now remains to find a convenient way of expressing the general path, i.e.,  $x_i(s_i)$ , which in turn will allow us to express  $\tilde{g}_i(s_i)$  using the relationship given above. Denman(1992) proposed a one-parameter family of paths specified as:

$$\rho_i^2 = \rho_{i0}^2 - \lambda^2 S_i^2$$

Where  $\rho_{i0}$  is the path's radius of curvature at the vertex. The parameter  $\lambda$  can be any value from zero to one. Some specials cases are:  $\lambda=0$  is a circular path,  $\lambda=\sqrt{\frac{\tilde{n}_i^2}{\left(\tilde{n}_i^2+1\right)}}$ 

describes an epicycloidal path with its base circle of radius ( $R_{i0}$ - $\rho_{i0}$ ) centered at the rotor center, and  $\lambda=1$  describes a cycloidal path. The tuning order of the path for each absorber is given as

$$\tilde{n}_{i} = \sqrt{\frac{R_{0} - \rho_{i0}}{\rho_{i0}}} \tag{2.33}$$

By considering the geometry of path, the expression for  $x_i(s_i)$  for the general absorber path can now be written as follows:

$$x_i(s_i) = 1 - \tilde{n}_i s_i^2 + \gamma_i s_i^4 + O(s_i^6)$$
 (2.34)

where

$$\gamma_i = \left(\frac{1}{12}\right) \left(\tilde{n}_i^2 + 1\right)^2 \left(\tilde{n}_i^2 - \lambda^2 \left(1 + \tilde{n}_i^2\right)\right)$$

#### 2.2.3.1 Analytical Results

It is now possible to seek approximate solution to the system's equations of motion (equation (2.31)), but first the terms have to be correctly ordered so that we can apply the method of averaging, which is the chosen solution technique.

Assume the ratio of the total absorbers inertia,  $I_0$ , to the rotor inertia, J, is small, we can define a small parameter  $\varepsilon$  such that

$$\varepsilon = b_0$$

We will restrict the analysis to study only harmonically oscillating torques and so we define  $\Gamma(\theta) = \Gamma_{\theta} \sin(n\theta)$  To quantify the nearness of the absorbers' tuning order,  $\tilde{n}_i$ , to the order of the applied torque, n, we introduce a mistuning parameter,  $\sigma_i$ , such that

$$\tilde{n}_i = n(1 + \varepsilon \ \sigma_i),$$

The other system parameters are scaled by  $\varepsilon$  as follows:

$$\mu_a = \varepsilon \ \widetilde{\mu}_a, \ \mu_0 = \varepsilon \ \widetilde{\mu}_0, \ \Gamma_0 = \varepsilon \ \widetilde{\Gamma}_0, \ \Gamma_a = \varepsilon^{3/2} \widetilde{\Gamma}_a, \ s_i = \varepsilon^{1/2} z_i$$
 (2.35)

with all the constant exponents of  $\varepsilon$  being fixed later. For small  $\varepsilon$ , the rotor speed can be expanded as follow (2.36)

$$v(\theta) = 1 + \varepsilon^{3/2} v_{3/2}(\theta) + HOT,$$

where HOT is higher order terms.

The path function can also be written in terms of  $\varepsilon$ :

$$\widetilde{g}_{i}(s_{i}) = 1 - \frac{\left(\widetilde{n}^{2} + \widetilde{n}^{4}\right)s_{i}^{2}}{2} + HOT$$

$$\gamma_{i} = \gamma_{0} + O(\varepsilon)$$
(2.37)

where

$$\gamma_0 = \left(\frac{1}{12}\right) (n^2 + 1)^2 (n^2 - \lambda^2 (1 + n^2))$$
 (2.38)

By substituting all the above scaled parameters into the equations of motion fro the previous section (equation (2.31)) we have:

$$vv'(\theta) = \varepsilon' \left\{ \frac{1}{N} \sum_{j=1}^{N} n^2 z_j + \widetilde{\Gamma}_{\theta} \sin(n\theta) \right\} + \frac{\varepsilon'^{+\nu}}{N} \sum_{j=1}^{N} 2n^2 z_j z_j' + HOT.$$
 (2.39)

and:

$$z_i'' + n^2 z_i = \varepsilon \left( 2\gamma_0 z_i^3 - 2n^2 \sigma_i z_i - \widetilde{\mu}_a z_i' - \frac{1}{N} \sum_{j=1}^N n^2 z_j - \widetilde{\Gamma}_{\theta} \sin(n\theta) \right) + HOT$$
 (2.40)

When a unison response occurs, all the absorbers have the same vibration amplitude,  $r_z$ , and phase,  $\phi_z$ . Using the method of averaging, and it's possible to find an approximate solution of the torque amplitude in terms of the absorber amplitude for the unison response, one obtains,

$$\widetilde{\Gamma}_{\theta} = 2n\sqrt{\left(\frac{\widetilde{\mu}_{a}}{2}r_{z}\right)^{2} + \left(\frac{3\gamma_{0}}{4n}r_{z}^{3} - n\left(\sigma + \frac{1}{2}\right)r_{z}\right)^{2}}$$
(2.41)

The second of the second of the second secon

By analyzing the stability of the unison response, the following results are obtained. For the bifurcation to a non-unison response,

$$r_{zbif} = \frac{4n}{\sqrt{54\gamma_0}} \left( 3\sigma - \left( (3\sigma)^2 - \frac{27}{4n^2} \left( n^2 \sigma^2 + \frac{\tilde{\mu}_a^2}{4} \right) \right)^{\frac{1}{2}} \right)^{\frac{1}{2}}$$
 (2.42)

For the jump condition,

$$r_{ij} \approx \frac{2n}{3} \sqrt{\frac{\sigma + \frac{1}{2}}{\gamma_0}}$$
 (2.43)

The correspondent torque levels for the bifurcation to non-unison and jump can be obtained by substituting equation (2.42) and equation (2.43) back into equation (2.41).

## 2.2.3.2 Numerical Examples

Based on the theoretical results just discussed, we now show how some of the solutions vary as a function of various system parameters. Unless otherwise stated, the following values are fixed and the path of the absorbers is always circular:

 $\varepsilon = 0.05$ , inertia ratio n = 2, order of applied fluctuating torque N = 2, number of absorbers  $\tilde{\mu}_a = 0.04$ , absorber damping  $\mu_0 = 0.05$ , rotor damping

Figure 2.14 shows the effect of mistuning on the amplitude of the absorber motion vs. applied varying torque level. It shows that the jump point occurs at higher torque levels as the level of mistuning is increased. From this plot we conclude that negative mistuning levels should be avoided. Related to this figure is Figure 2.15 that shows

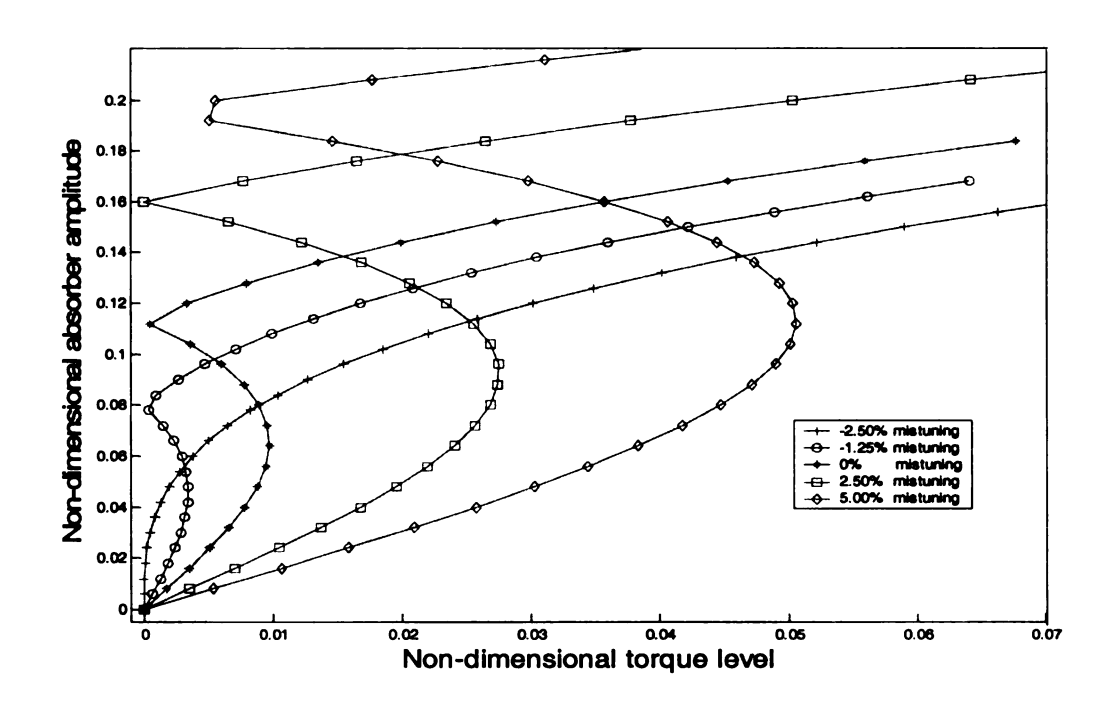


Figure 2.14 Effect of mistuning on amplitude of absorber motion vs. applied varying torque level,  $r_z$  vs.  $\Gamma_{\theta}$ 

the corresponding behavior of the rotor acceleration. It should be noted tht not all the same mistuning levels have been plotted, but the line for the locked absorbers has been added. For any curve below this line the absorbers are reducing the vibration, whereas if the response curve lies above the line, the absorbers are adding to the vibration problem.

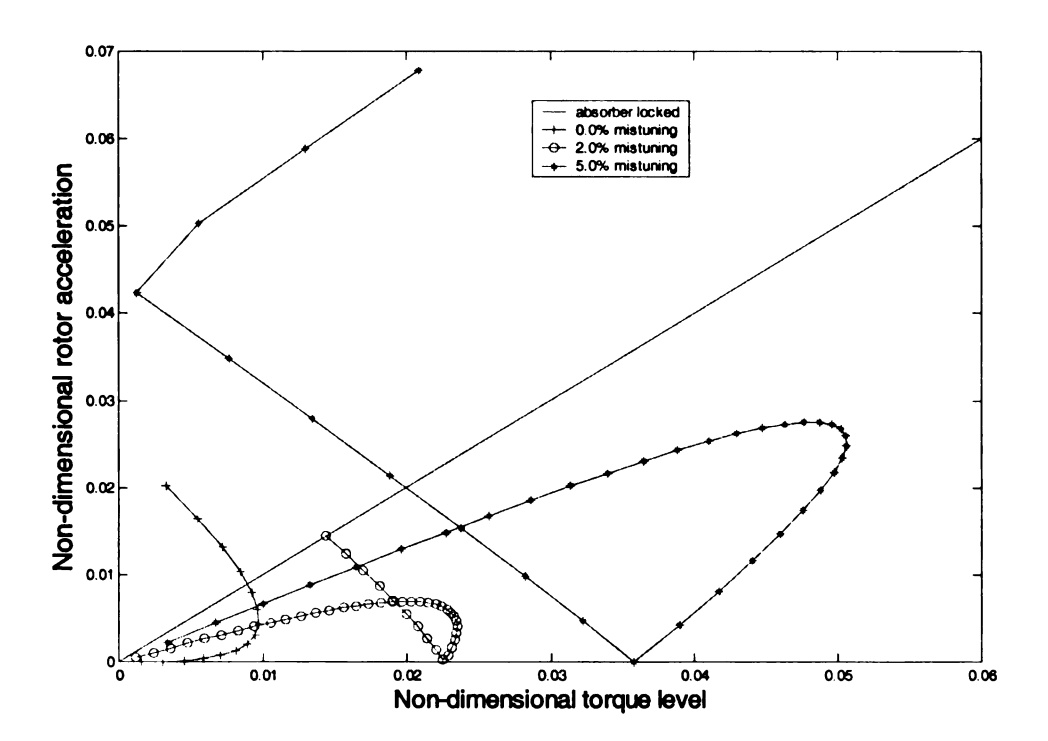


Figure 2.15 Amplitude of the non-dimensional rotor acceleration vs. the applied torque level, vv' vs.  $\Gamma_{\theta}$ 

Figure 2.16 shows the two different critical torque levels versus the mistuning level. One is associated with the unison motion becoming unstable and the other with jump. These are obtained by substituting equation (2.42 and 2.43) into the equation (2.41), respectively.

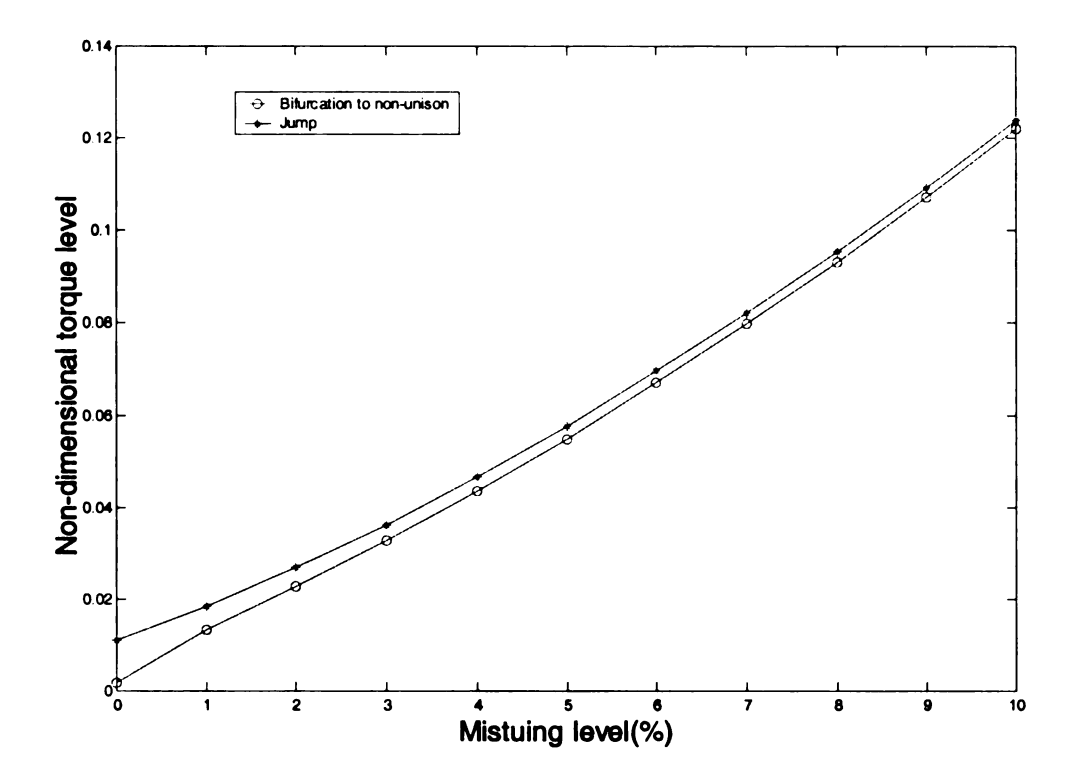


Figure 2.16 Critical torque levels vs. the mistuning level for bifurcation to non-unison and jump,  $\Gamma_{\theta}$  vs.  $\varepsilon\sigma$ 

Finally, Figure 2.17 shows non-dimensional rotor acceleration normalized by the applied varying torque, versus varying torque frequency. Here one can see the effect of the nonliearity. As the torque level increases, the minimum point moves to the left (compare this linear theory result of Figure 2.6. where the minimum point is not a function of the level of the torque). Moreover, the response curves become multivalued as the torque level and /or torque frequency changes, i.e., jumps can occur.

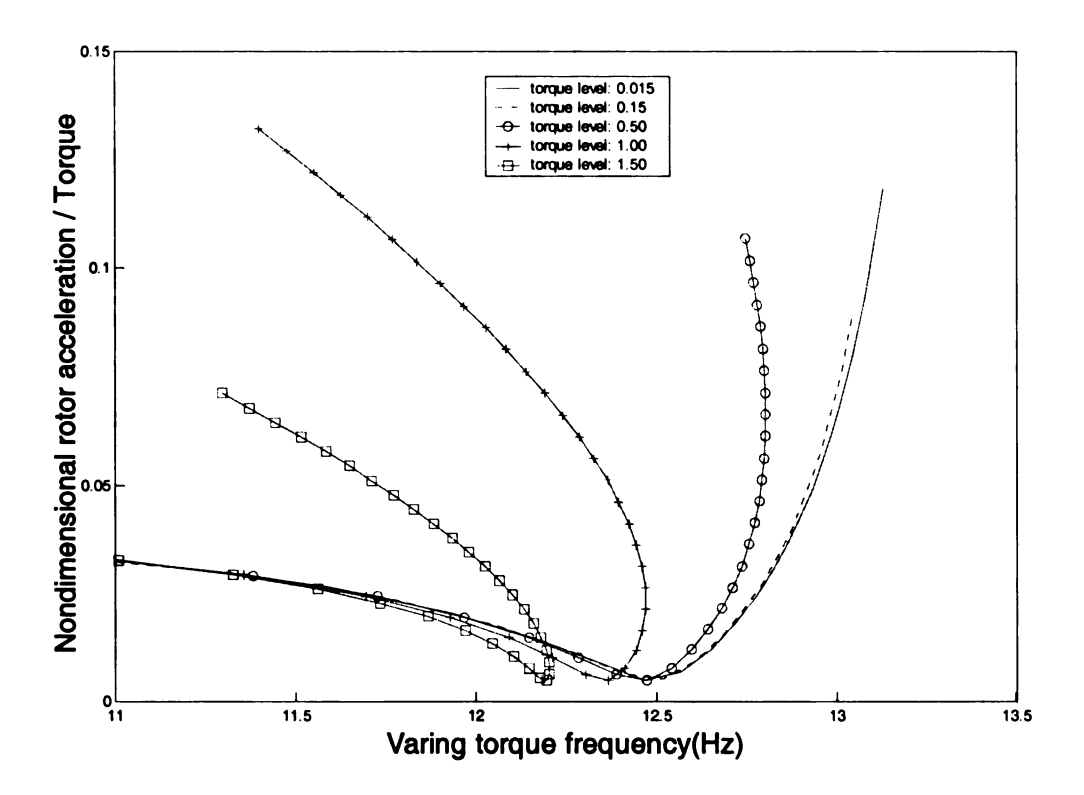


Figure 2.17 Rotor system frequency response, non-dimensional rotor acceleration over applied varying torque, versus varying torque frequency ( $vv'/\Gamma_{\theta}$  vs.  $n\Omega=\omega$ )

## **CHAPTER 3**

# **Experimental Setup**

In this chapter the experiment facility is described. Only an overview is presented, with more details given in Appendix B and Appendix C.

### 3.1 Experiment Facility

Figure 3.1 shows a general view of the experimental facility, while Figure 3.2 presents a schematic diagram of its major components. The motor, a Bulletin Nr. 1326 AR AC servomotor, is used to turn a flywheel that the absorbers are attached to. The motor has its own controller, a Bulletin 1391 AC PWR Servo Controller that can be configured to control the torque applied to the motor. A torque transducer, a SensorData T360-106, is installed on the shaft to measure the actual applied torque. There is an encoder attached to the shaft that generates 1000 pulses per revolution. A frequency-to-voltage converter, made by Dynapar Corp., is used to convert these pulses to a signal proportional to the shaft speed. In addition to generating this signal, the frequency-to-voltage converter outputs a +5V signal at a pre-determined speed. This is used as a safety feature and will trigger a motor shut-down if the motor speed goes above this set value. The AD-3525 FFT Analyzer is used to measure the motor speed and torque in both the frequency and time domain.

Finally, a WaveTek Model 75 arbitrary wave-form generator is used to create an oscillatory signal,  $A\sin(n\theta)$ , where n is typically chosen to be close to the order of the

CPVA. The angular position of the shaft,  $\theta$ , is obtained from the encoder and is used as the external time base for the wave-form generator. The oscillatory signal is then added to another signal that generates the constant mean speed,  $\Omega$ , of the shaft. The details of how this  $\Omega$  component of the signal is generated are presented in the next section.

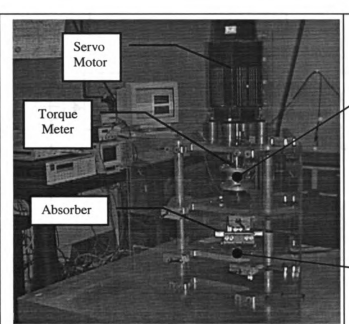


Figure 3.1 General view of the test facility.



Figure 3.2(a) Test facility partially disassembled, showing main shaft with flywheel/absorber attachment point.



Figure 3.2(b) Absorber mass showing bifilar attachment. This is bolted to block shown in (a)

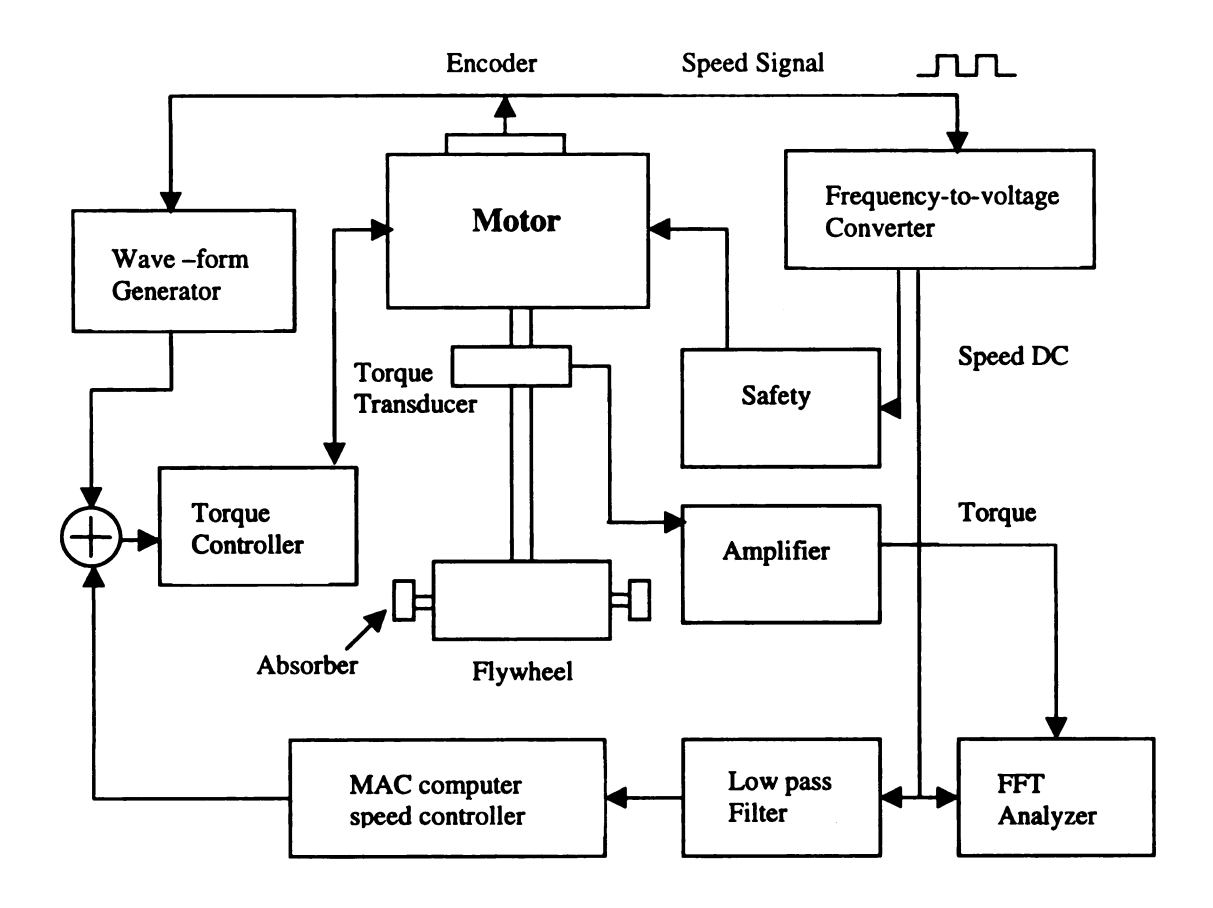


Figure 3.3 Experiment system block diagram

### 3.2 Motor Mean Speed Controller

Experimentally it was found that even when a constant control signal was input to the torque controller (i.e., the fluctuation signal Asin( $n\theta$ ) was zero) the resulting speed of the motor would drift slightly from the desired speed,  $\Omega$ . To counter this, an additional speed controller was used, designed specially to maintain the desired mean speed at a fixed level without altering the higher frequency speed fluctuations that arise on account of the fluctuating input signals when they are added back in. This was accomplished by first filtering the actual speed of motor by a low pass filter (set to 1Hz). The signal was then sampled using LabView software running on a Macintosh computer. A program was written to compare this to the desired speed and a PI control loop used to generate the necessary value for the input to the torque controller. We were thus able to fix the mean speed of the motor by generating the required torque input signal. As can be seen from the schematic of Figure 3.3, the Asin( $n\theta$ ) signal created by the wave-form generator is added to this signal before they both are passed to the torque controller.

## **CHAPTER 4**

## **Experimental Results**

A variety of experiments were conducted using two absorbers moving along circular paths. The influence of absorber tuning, torque level, torque frequency and mean speed rate were all investigated and compared to theoretical predictions. Before this comparison could be made, the relationship between the actual physical parameters of the system and the corresponding theoretical, non-dimensional terms used in the theory had to be made. A tabulated summary of these relationships are presented in the next section. This is followed by a presentation and discussion of the results from the experiments. More specific details of how the system parameter values were obtained, how instruments were calibrated and tested, and what the coefficients were to convert measured signal strength to physical units can be found in Appendix C.

#### **4.1 System Parameters**

We carefully measured the CPVA's parameters, such as the dimensions of the rotor, absorber cord length, absorber mass etc. Table 4.1 shows all of these parameters and their description. Their relationship to the terms used in the publication by Alsuwaiyan and Shaw (1999) is also listed.

It is important to compare the experimental results with the theoretical solutions and so the relationships between the actual physical variables and their non-dimensional counterparts are given in Table 4.2.

Table 4.1 CPVA notation and system parameter values

Item	Description	Value
R	Distance between flywheel center and the point	0.1583m
	around which absorber rotates	
r	Radius of absorber movement relative to the	25.3mm (depends on
	flywheel	CPVA order)
ñ	CPVA internal order $\tilde{n} = \sqrt{\frac{R}{r}}$	2.50 (but can be changed)
n	External excitation order	Depends on the frequency
	$\widetilde{n}=n(1+\varepsilon\sigma)$	of the applied torque
$R_{0}$	Distance between flywheel center and absorber	0.1836m (depends on
	$C.G. R_0 = R + r$	CPVA order)
J	Flywheel inertia (EXCLUDE absorbers)	0.1658Kg*m <sup>2</sup>
m	Absorber mass	0.330Kg
N	Number of absorbers	2
$m_0$	Total absorber mass	0.660Kg
$I_{0}$	Absorber inertia $I_0 = NmR_0^2$	0.0222Kg*m² (depends on CPVA order)
$b_0$	Ratio of the inertia of the absorbers to the	0.134 (depends on CPVA
	flywheel, $b_0 = \frac{I_0}{J}$	order)
ε	Ratio of the absorbers inertia to the rotor inertia	0.134 (depends on CPVA
	$\varepsilon^p = b_0(p=1)$	order)
$\gamma_{0}$	Absorber path parameter (circular path)	
	$\gamma_0 = \frac{1}{12}(n^2 + 1)^2 n^2$	
Ω	Rotor mean speed (rad/s)	
$f_0$	Rotor mean speed (Hz)	
$f_{\tilde{n}}$	CPVA natural frequency $f_{\tilde{n}} = f_0 \tilde{n}$	
$f_n$	External varying torque frequency $f_n = f_0 n$	
	$f_{\tilde{n}} = f_n(1 + \varepsilon \sigma)$	
σ	Mistuning $\sigma = \frac{1}{\varepsilon} (\frac{\tilde{n}}{n} - 1) = \frac{1}{\varepsilon} (\frac{f_{\tilde{n}}}{f_n} - 1)$	

Table 4.2 Relationship between the actual physical variables and their non-dimensional counterparts

Item	Physical Meaning	Non-dimensional	Experimental
$T_{\theta}$	Amplitude of the varying applied torque	$\Gamma_{\theta} = \frac{T_{\theta}}{J\Omega^{2}} = \varepsilon^{\frac{3}{2}} \tilde{\Gamma}_{\theta}$ $\tilde{\Gamma}_{\theta} = \frac{1}{\varepsilon^{\frac{3}{2}}} \Gamma_{\theta} = \frac{1}{\varepsilon^{\frac{3}{2}}} \frac{T_{\theta}}{J\Omega^{2}}$	$T_{\theta} = J\Omega^{2}\Gamma_{\theta} = \varepsilon^{\frac{3}{2}}J\Omega^{2}\widetilde{\Gamma}_{\theta}$
T <sub>0</sub>	Mean applied torque	$\Gamma_0 = \frac{T_0}{J\Omega^2} = \varepsilon \ \tilde{\Gamma}_0$ $\tilde{\Gamma}_0 = \frac{1}{\varepsilon} \Gamma_0 = \frac{1}{\varepsilon} \frac{T_0}{J\Omega^2}$ $v = \frac{\dot{\theta}}{\Omega}$	$T_0 = J\Omega^2 \Gamma_0 = \varepsilon \ J\Omega^2 \widetilde{\Gamma}_0$
$\dot{\theta}$	Flywheel angular velocity (including mean speed)	$v = \frac{\dot{\theta}}{\Omega}$	$\dot{ heta} = v\Omega$
$\ddot{\theta}$	Flywheel acceleration	$vv' = \frac{1}{\Omega^2}\ddot{\theta}$	$\ddot{ heta} = \Omega^2 v v'$
Ca	Absorber damping	$\mu_a = \frac{c_a}{m\Omega} = 2\xi n$	$c_a = m\Omega\mu_a = 2\xi mn\Omega$
$c_0$	Flywheel damping	$\mu_0 = \frac{c_0}{J\Omega}$	$c_0 = J\Omega\mu_0$
$\frac{\ddot{ heta}}{T_{ heta}}$	System response (flywheel acceleration / torque)	$\frac{\ddot{\theta}}{T_{\theta}} = \frac{1}{J\varepsilon^{\frac{3}{2}}} \frac{vv'}{\tilde{\Gamma}_{\theta}}$	$\frac{\upsilon\upsilon'}{\widetilde{\Gamma}_{\theta}} = J\varepsilon^{\frac{3}{2}}\frac{\ddot{\theta}}{T_{\theta}}$
S	Absorber amplitude(arc length)	$s = \frac{S}{R_0} = \varepsilon^{\frac{1}{2}} r_z$ $r_z = \frac{S}{R_0} \varepsilon^{-\frac{1}{2}}$	$S = R_0 \varepsilon^{\frac{1}{2}} r_z$

## **4.2 CPVA System Frequency Response Experiments**

## 4.2.1 System Frequency Response when Absorbers are Locked

We locked the two absorbers and ran the motor with a mean speed of 300RPM. The applied torque was held constant at 0.25Nm.

#### 4.2.1.1 Results

By changing the frequency of the applied torque, we obtain the frequency response of the system shown in Figure 4.1.

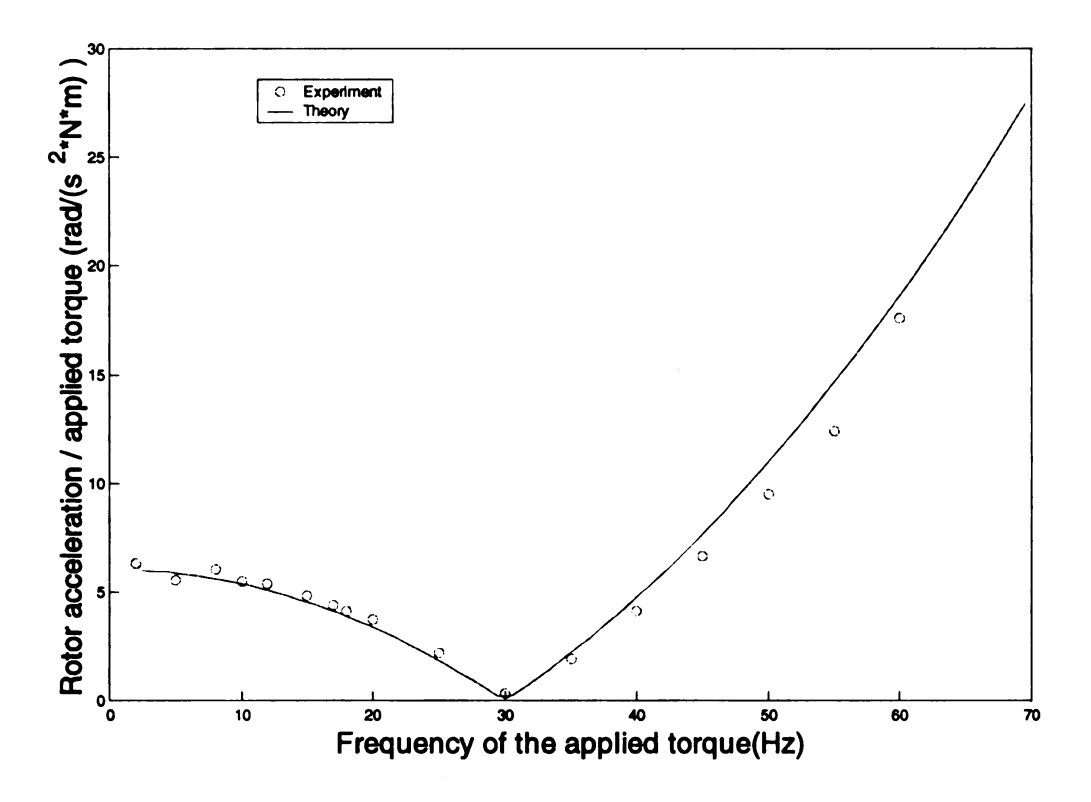


Figure 4.1 System frequency response with the absorbers locked,  $T_{\theta}$ =0.25Nm, and mean speed =300RPM

#### 4.2.1.2 Discussion

Figure 4.1 shows that when the absorbers are locked, the system itself acts like a torsional vibration absorber. This is due to the flexibility in the shaft as was

discussed in Section 2.2.2. By fitting the experimental results to the theoretical solution (A2) using equation (A2) in Appendix A, we can estimate the moments of inertia  $I_1$  and  $I_2$  and the spring constant of the shaft. The estimated values are:  $I_1 = 0.0013 \text{Kg m}^2$ ,  $I_2 = 0.1645 \text{ Kg m}^2$  and K = 5846 Nm/rad.

## 4.2.2 Linear System Frequency Response when Absorbers are Free

We activate the two absorbers and set the cord length to 25.3mm. Using equation (2.19), the expected CPVA order is 2.5. The rotor mean speed is still 300RPM.

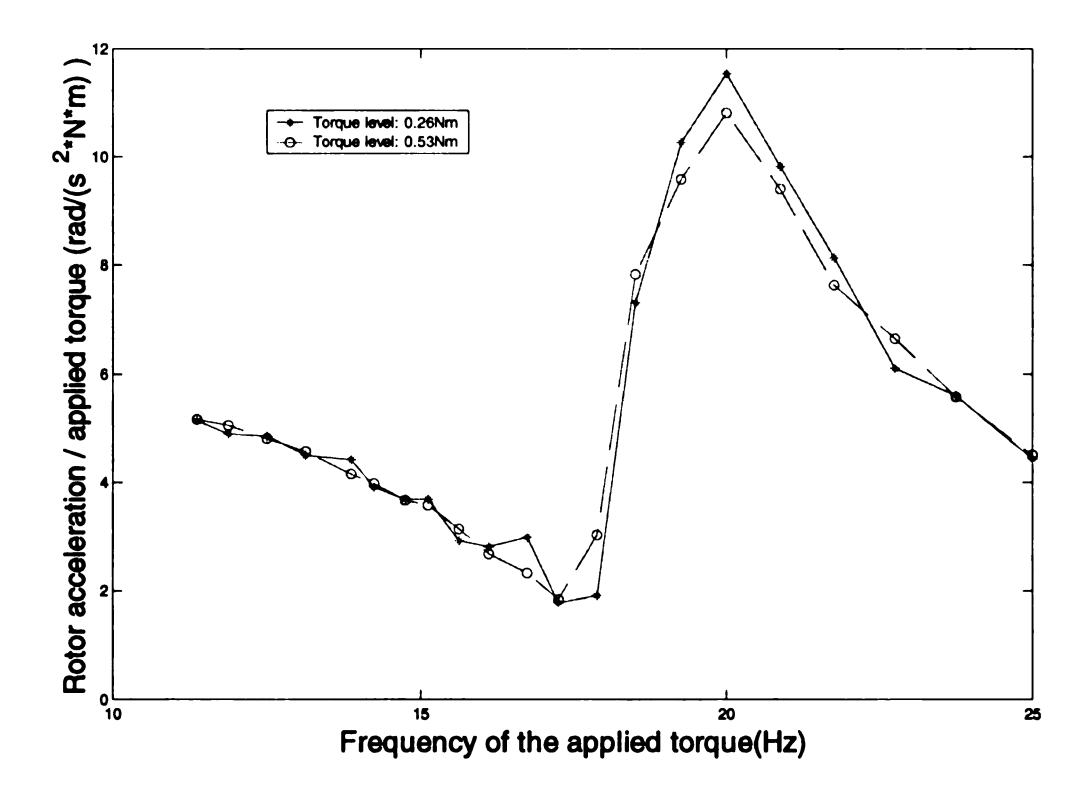


Figure 4.2 System frequency response when absorbers are free for two different torque levels:  $T_0=0.26Nm$  and 0.53Nm

#### 4.2.2.1 Results

The level of the applied torque was decreased, until two successive responses converged, i.e., a linear behavior had been found. The two torque levels were  $T_0$ =0.53Nm and 0.26Nm. The results are plotted in Figure 4.2.

#### 4.2.2.2 Discussion

Since the experimental system responses are both in the linear region, we can use the 3-DOF linear CPVA theoretical model (details in Section 2.2.2) to fit the experimental results. Figure 4.3 shows this result. The estimated values of the CPVA order and damping ratio are:  $\tilde{n} = 3.5$  and  $\xi = 8.0\%$  respectively.

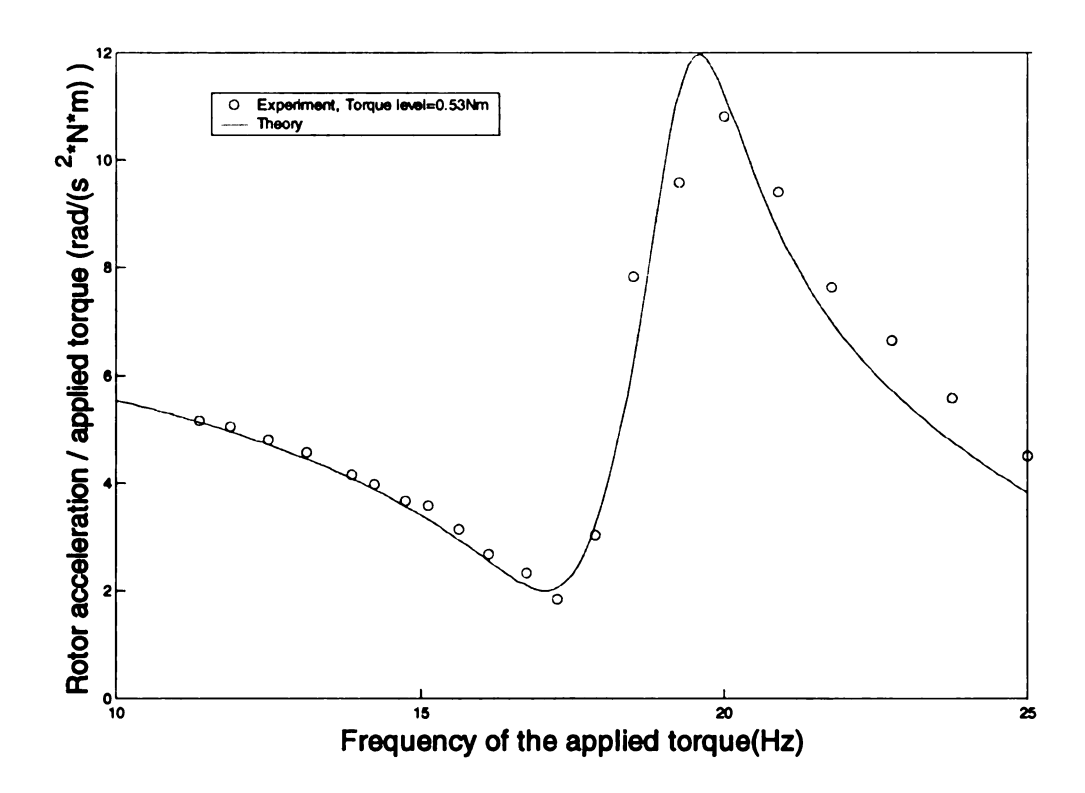


Figure 4.3 System frequency response when absorbers are free with torque level 0.53Nm. Theory fit from equation (2.26) using 3-DOF CPVA model.

The estimated experimental CPVA order of 3.5 is much larger than the theoretical value of 2.5. The actual cord length, r, is 25.3mm. If the CPVA order is 3.5, the string length should be 12.9mm. Many different studies were completed to explain this discrepancy, but no good reason could be found. Details are given in Appendix D.

## 4.2.3 System Frequency Response at Different Torque Levels

The two absorbers are free, the cord length is 25.3mm, and the mean speed is 300RPM.

#### 4.2.3.1 Results

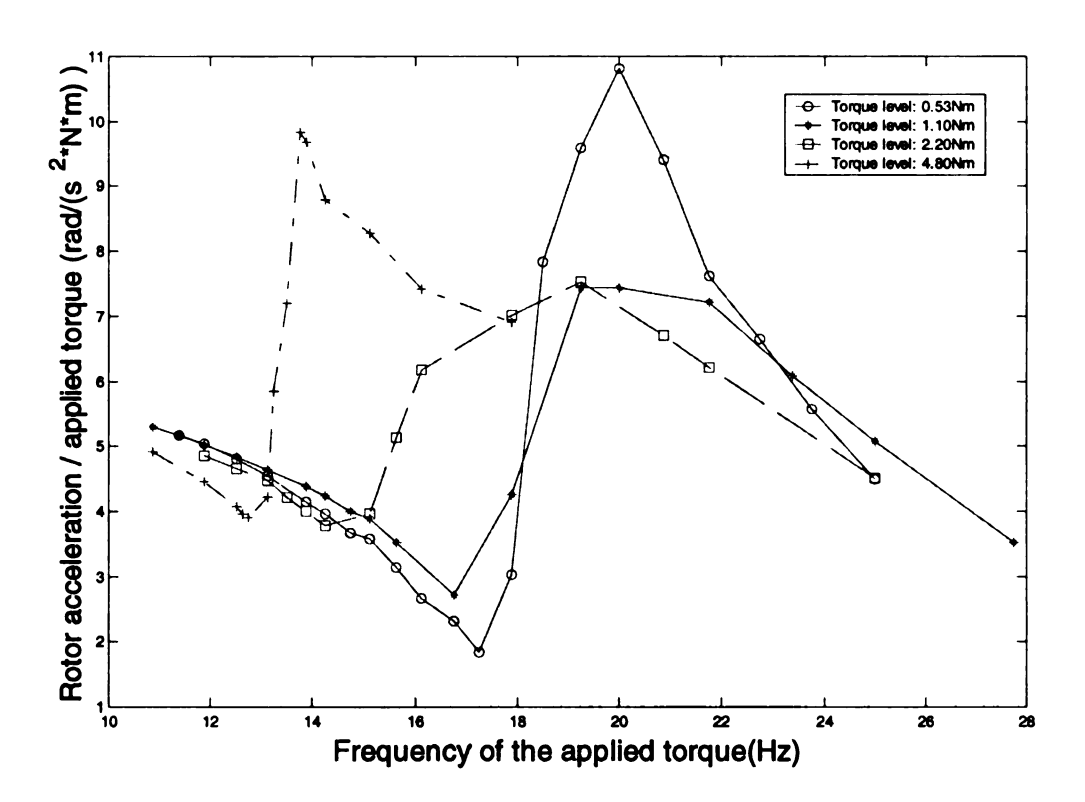


Figure 4.4 System frequency response when absorbers are free for four different torque levels: 0.53Nm, 1.10Nm, 2.20Nm and 4.80Nm

Figure 4.4 shows the system frequency response curves for different torque levels: 0.53Nm, 1.1Nm, 2.2Nm and 4.8Nm.

#### 4.2.3.2 Discussion

The form of the frequency response curves for torque levels of 1.1Nm and 2.2Nm are different from the other two curves. The resonance peak is much reduced. However, this may be due to a lack of data values in the neighborhood of 17-19Hz. More importantly, the trend of the minimum point moving to the left as the torque is increased fits well with nonlinear theory (see Figure 2.17). However, there are two problems that are not apparent at first. It seems that there must be an additional type of damping present that is not modeled in the theoretical section. With reference to Figure 2.17, the "height" of the minimum point should not change with increased torque level. In our case it does. The second problem arises if one carefully converts the physical values of applied torque into the non-dimensional form and then uses the nonlinear theoretical model (Section 2.2.5) to predict the response, the theoretical response curves associated with torque levels of 0.53Nm to 4.8Nm are indistinguishable. This would indicate that, theoretically, we are still operating in the linear region.

## 4.2.4 System Frequency Response with Different Rotor Mean Speeds

The absorber string cord length is 25.3mm and the rotor mean speed is 150RPM.

#### 4.2.4.1 Results

Figure 4.5 shows the system frequency response with the absorbers locked and with the absorbers free. Applied torque is 0.50Nm in both cases.

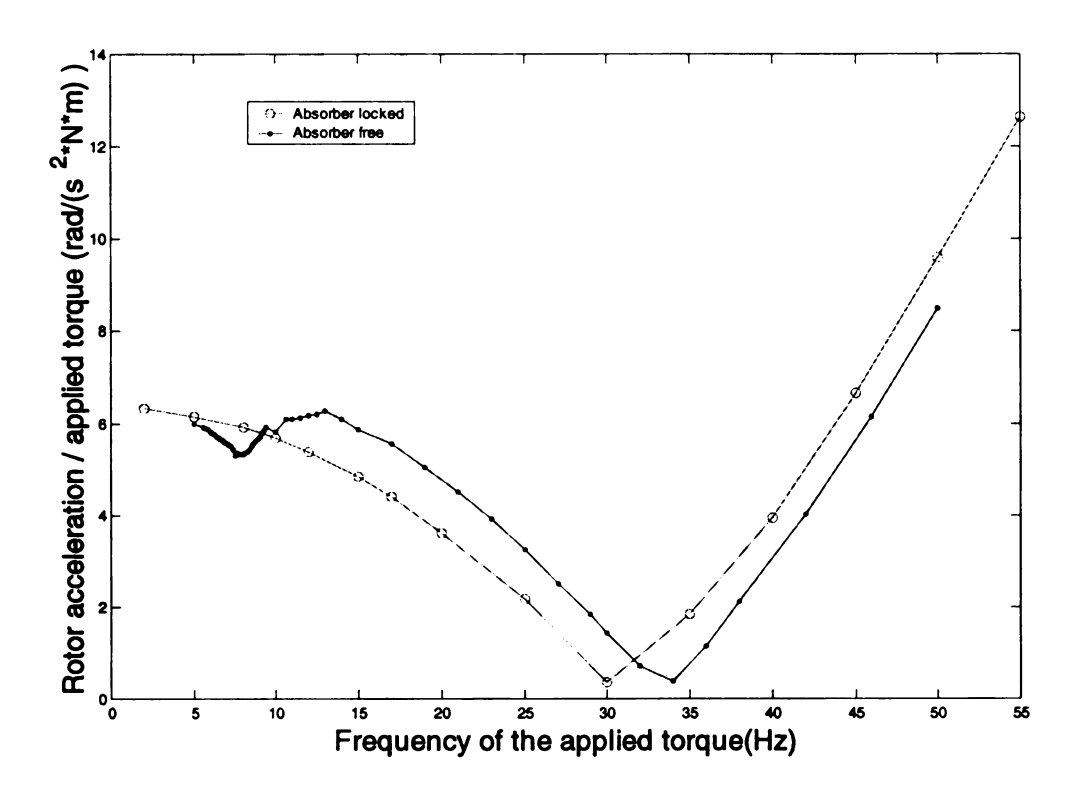


Figure 4.5 System frequency response when absorbers are locked and absorbers are free with 150RPM mean rotor mean and 0.50Nm applied torque

## 4.2.4.2 Discussion

By using the 3-DOF linear CPVA model to fit the experiment data, the estimated values of the CPVA order and damping ratio are:  $\tilde{n} = 3.0$  and  $\xi = 8.5\%$  respectively. The error between the expected CPVA order and the experimentally estimated one is less than that when the rotor mean speed was 300RPM.

## 4.2.5 System Frequency Response with Different Absorber Cord Length

We changed the string cords length to 40.5mm and thus the CPVA order should change to 1.98.

## 4.2.5.1 Results

For a mean speed of 300RPM and an applied torque 0.50Nm, the system frequency response is shown in Figure 4.6.

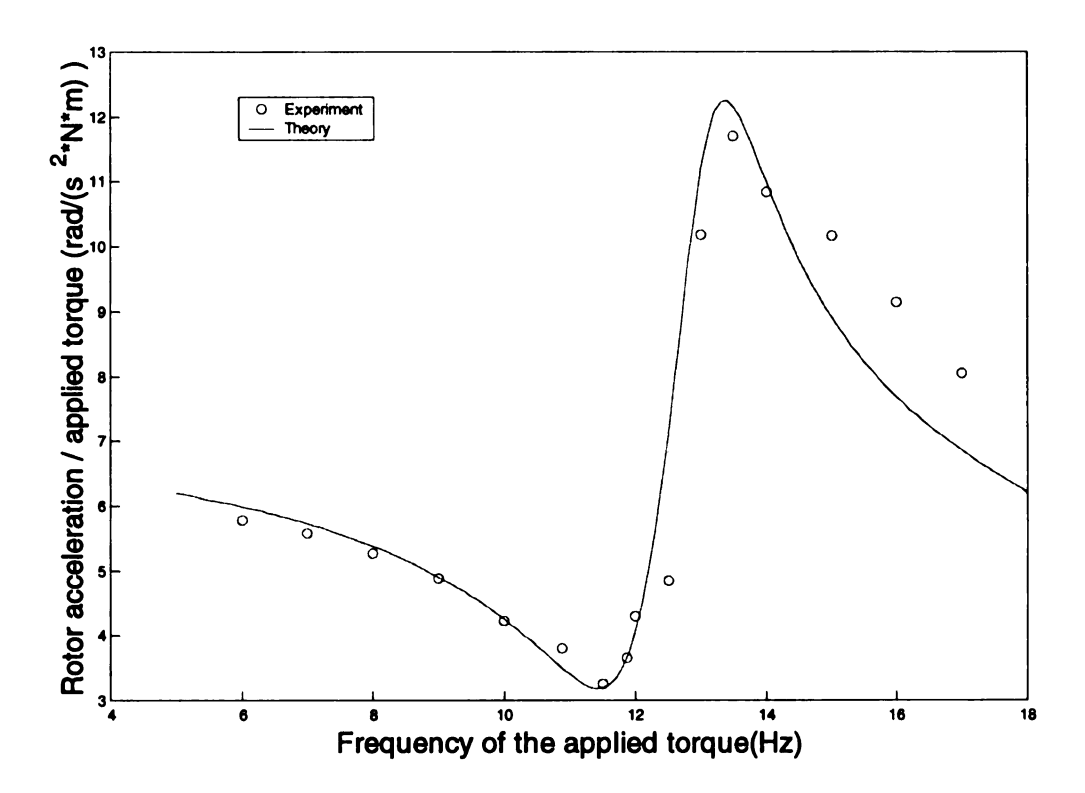


Figure 4.6 System frequency response when absorbers are free (cord length is 40.5mm) with torque level 0.50Nm. Theory fit from equation (2.26) using 3-DOF CPVA model.

## 4.2.5.2 Discussion

By using the 3-DOF linear CPVA model to fit the experiment data, the estimated values of the CPVA order and damping ratio are:  $\tilde{n} = 2.3$  and  $\xi = 7.0\%$  respectively. If the CPVA order is 2.3, the cord length should be 29.9mm.

## **4.3 CPVA Bifurcation and Mistuning Experiments**

#### 4.3.1 Locked Absorbers

We locked the two absorbers and run the rotor at 300RPM mean speed with the frequency of the applied torque held constant at 12.5Hz. The applied torque level was changed and we recorded the rotor acceleration. The results are shown in Figure 4.7. The plot is a straight line as would be expected. This will be used as a baseline comparison for the experiments to follow where the absorbers will be unlocked.

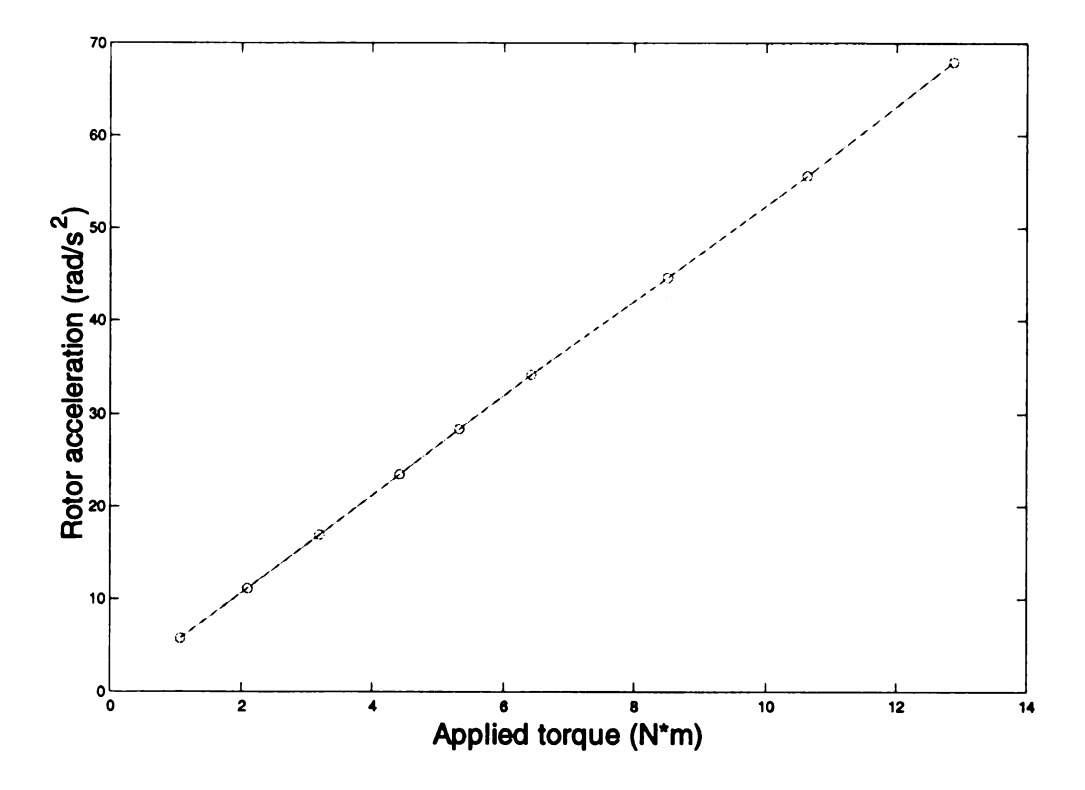


Figure 4.7 Rotor acceleration vs. applied torque when absorbers are locked

## **4.3.2 Bifurcation Experiment**

We unlocked the absorbers and run the rotor at 300RPM mean speed. The absorber cord length was 25.3mm and the applied torque frequency was 12.5Hz.

#### 4.3.2.1 Results

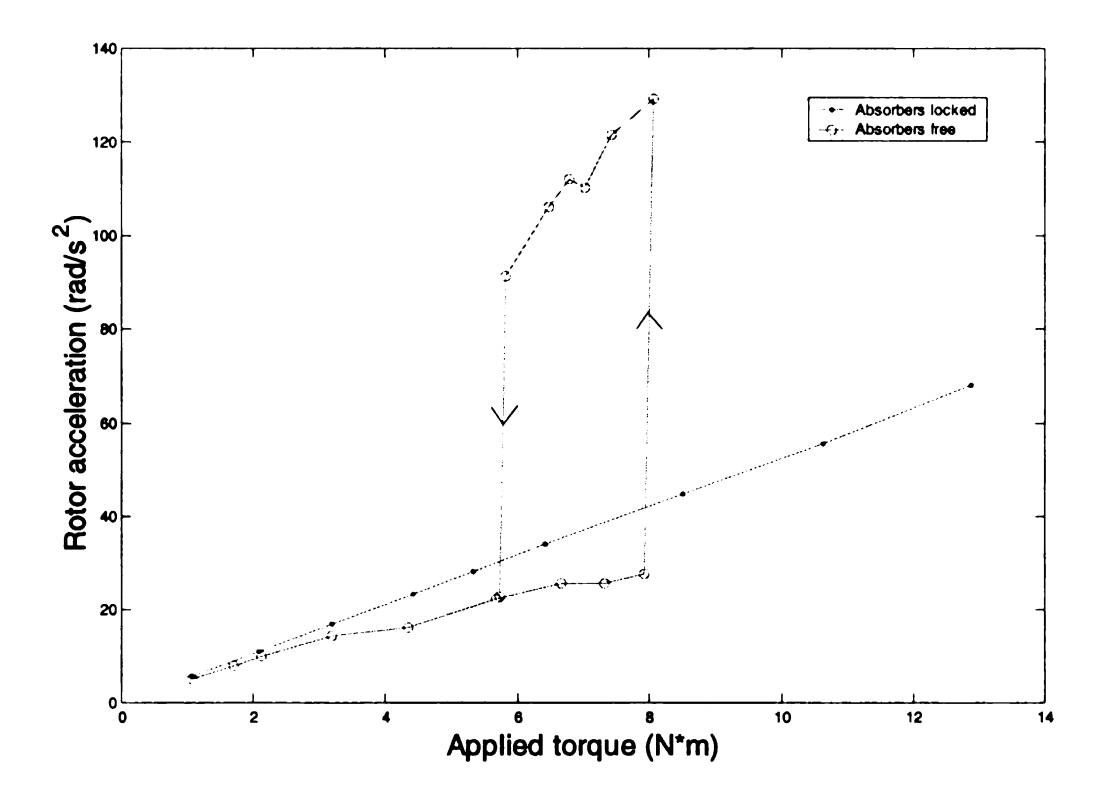


Figure 4.8  $|\ddot{\theta}|$  vs.  $T_{\theta}$  experimental results for locked and unlocked absorbers. The applied torque frequency is 12.5Hz

Starting from 1.07Nm, the applied torque was gradually increased. We found that the rotor acceleration also increased gradually. When the applied torque reached 8.07Nm, the acceleration suddenly jumped from 27.6rad/s<sup>2</sup> to 129rad/s<sup>2</sup>. If the applied torque is then decreased, the rotor acceleration remains high until the torque is decreased to 5.73Nm, at which point the rotor acceleration jumps back down. The experimental results are shown in Figure 4.8.

#### 4.3.2.2 Discussion

Figure 4.8 clearly shows that the CPVA response bifurcates when the applied torque is increased to 8.07Nm. In order to compare the experimental result with the theoretical solution, we transform the experimental data into non-dimensional form (see Table 4.1&2). Figure 4.9 shows the experimental and the theoretical results superimposed. The theoretical curve comes from the non-linear CPVA analytical results of Section 2.2.5 with parameter values consistent with the experimental values found throughout this chapter, i.e.,  $\tilde{n} = 3.5$  and  $\xi = 8.0\%$ .

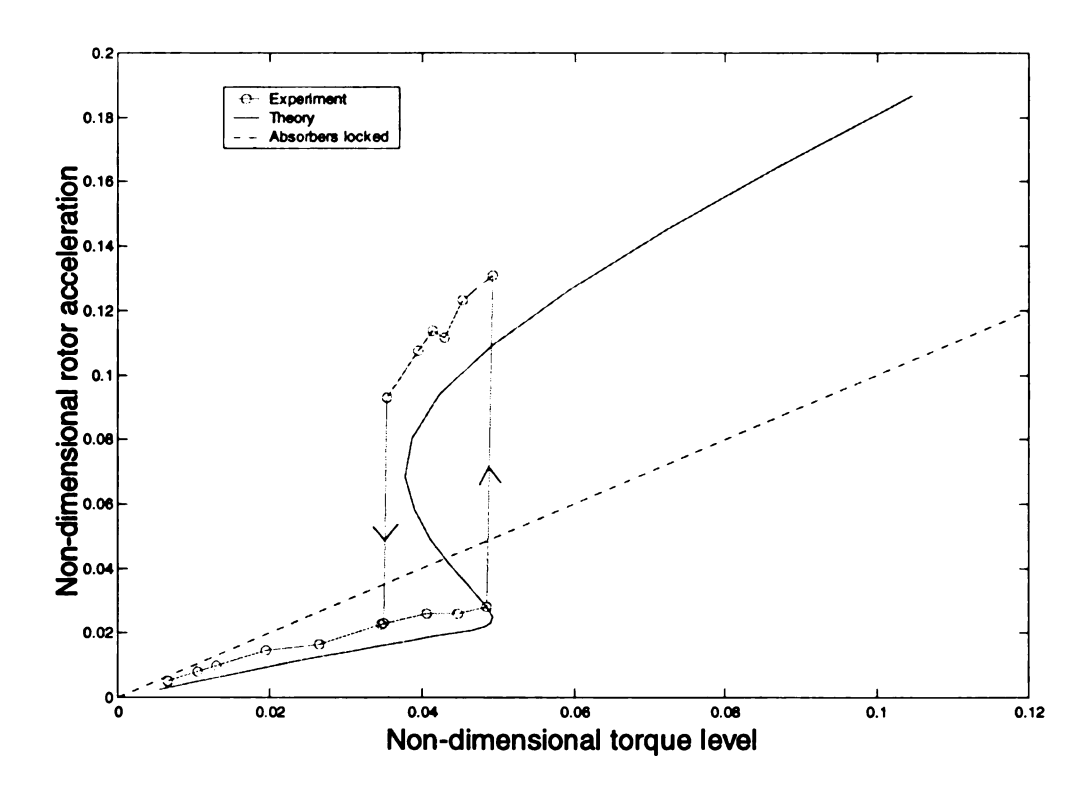


Figure 4.9 vv' vs.  $\Gamma_{\theta}$  comparing theoretical and experimental results. The applied torque frequency is 12.5Hz

If we assume the CPVA order is 3.5, it's interesting to find that the 2.4% mistuning level theory curve fits the experiment data well. However, the actual

applied torque frequency is 12.5Hz, which represents a 40% mistuning level if the CPVA order is 3.5. Clearly there is some discrepancy between the theory and the experimental results.

## 4.3.3 Bifurcation Experiments at Various Mistuning Levels

We repeat the experiments of Section 4.3.2 but now carry-out the torque sweeps at different levels of forcing frequency. The forcing frequency,  $f_n$ , is related to the detuning parameter,  $\sigma$ , discussed in Alsuwaiyan and Shaw (1999) (and see Table 4.1).

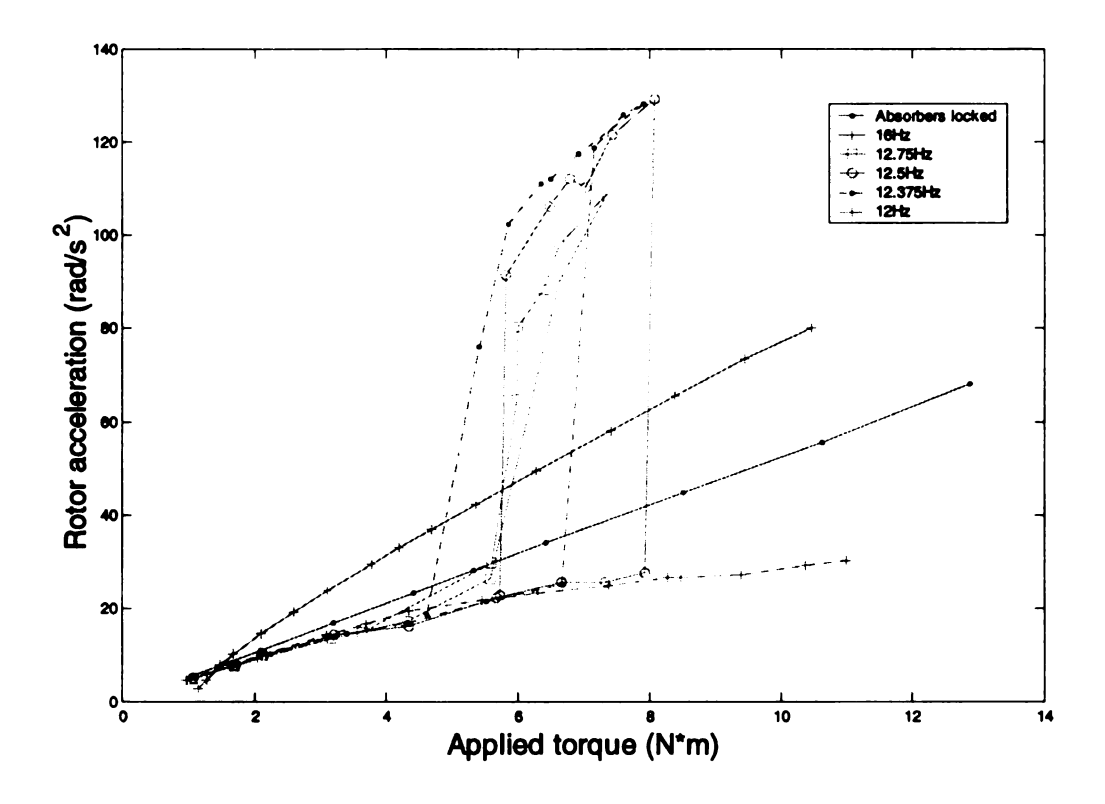


Figure 4.10  $|\ddot{\theta}|$  vs.  $T_{\theta}$  showing bifurcation points for different applied torque frequencies

## 4.3.3.1 Results

We ran 8 groups of experiments with different applied torque frequencies: 16Hz, 15Hz, 14Hz, 13Hz, 12.75Hz, 12.5Hz, 12.375Hz and 12Hz. The bifurcation torque for 16Hz is very small compared to that of 12.5Hz. The bifurcation torque for 12Hz is equal or larger than 10.99Nm, because when we increased the torque level to 10.99Nm, the experiment had to be stopped as one of the absorber cords broke. Figure 4.10 shows the experimental data associated with some of the frequencies and Figure 4.11 shows all of the critical values of the applied torque at which the jumps occur.

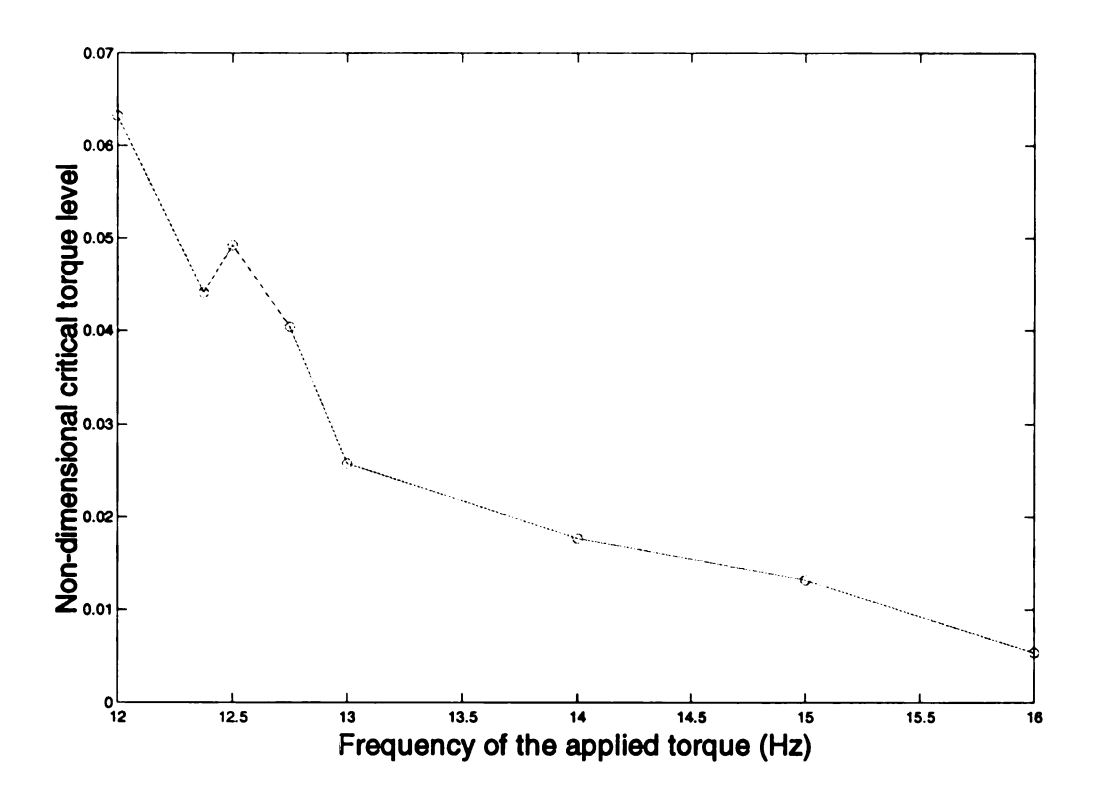


Figure 4.11 Non-dimensional critical torque level vs. frequency of the applied torque

## **CHAPTER 5**

# **Concluding Remarks and Recommendations for Future Work**

In this thesis we focused on designing and executing experiments to investigate the linear and nonlinear behavior of a CPVA. The experimental apparatus has been well tested and calibrated. The system parameter values and their relationship to the nondimensional quantities used in previously published works have been carefully documented. This has allowed for a direct comparison between theoretical predictions and experimental results to be made. By in large this comparison shows good agreement with the exception of two important discrepancies. The first is that the predicted tuning order of the absorber is different from the measured value and the second is that some of the nonlinear effects that are observed in the experiment should, theoretically, not be occurring until larger values of torque are applied (see Section 4.2.3). An exhaustive search into the reason behind these discrepancies has been made and is documented in Appendix D. Great care has been taken to accurately measure the parameters of the system and to independently measure the applied torque and angular velocity of the rotor. Hence, it is concluded that there is a mechanism present in the system that is not modeled by the theory that is causing the discrepancies. Candidates may be a more complicated type of damping, such as friction, or additional degrees of freedom that cause additional resonances and anti-resonances.

The priority for future work must focus on uncovering the reason(s) behind the two problems outlined above. More specifically, the following should be addressed:

- Instrument the absorbers so that their displacements can be measured.
- Run tests in what is believed to be linear and nonlinear regions and measure the
  corresponding displacements of the absorbers. Conclude if the drift in the minimum
  point seen in Figure 4.4 is indeed due to nonlinearities i.e., large absorber
  displacements.
- Measure the absorber damping while the system is rotating. Perhaps by suddenly removing the torque oscillations and the torque feedback control and observing the decay in the absorber motion.
- Simplify the drive to the flywheel by removing the torque meter and the associated coupler. This will aid in minimizing any misalignment problems and will increase the shaft stiffness. The torque can still be measured via the current in the servomotor.
- If necessary, redesign the way the absorbers are attached to the rotor. For example a rigid link mechanism may be better or cords "clamped" at both ends instead of allowing the cord to rotate and rub around a pin.
- The addition of the MAC computer feedback system may alter the dynamics of the system. It should be disconnected to check this.

In addition to these recommendations, it remains to study the behavior of absorbers moving along non-circular paths, increasing the number of absorbers to four (to study non-unison responses), and to study the response due to different forms of torque input.

# **APPENDICES**

## **APPENDIX A**

### **Linear Torsional Vibration Absorber**

We wish to show that the lower disk can act as a torsional vibration absorber for the upper disk, which has a moment of inertia  $I_1$ .

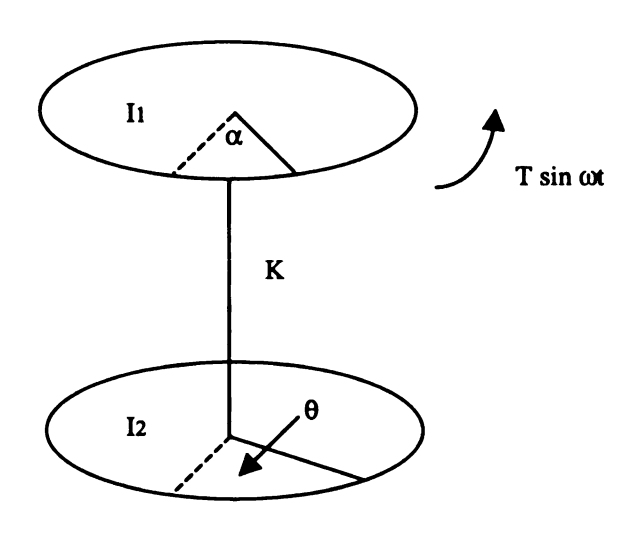


Figure A.1 Linear torsional vibration absorber

The equations of motion of the system shown in Figure A.1 are

$$I_{1}\ddot{\alpha} + K(\alpha - \theta) = T \sin \alpha t$$

$$I_{2}\ddot{\theta} + K(\theta - \alpha) = 0$$
(A1)

where I<sub>2</sub> is the total inertia of all the components rotating with the lower disk.

The steady state response of the disk 1 can be written as

$$\alpha_0 = \frac{\left(\omega^2 I_2 - K\right)}{\left(\omega^2 I_2 - K\right)\left(\omega^2 I_1 - K\right) - K^2} T \tag{A2}$$

This is sketched in Figure A2.

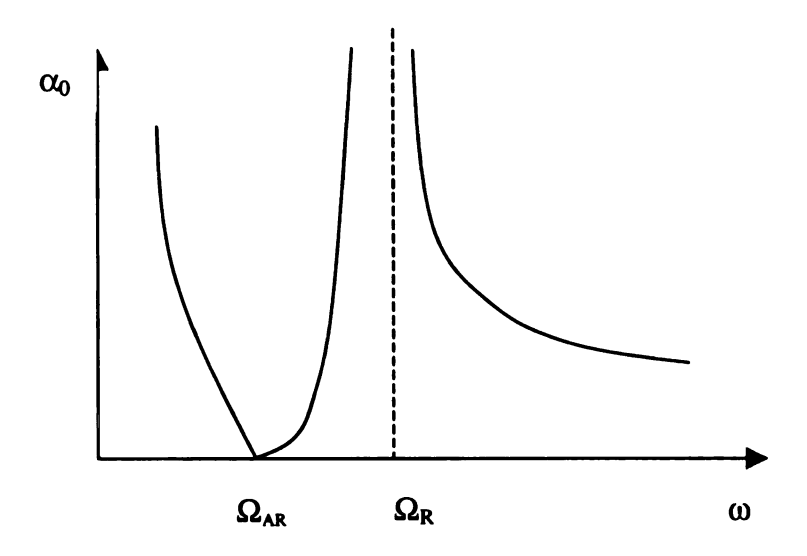


Figure A.2 System response of disk 1

At the special frequency  $\Omega_{AR} = \sqrt{K/I_2}$ , the disk 1 rotation will be zero.

## APPENDIX B

## **Procedure to Start-up the CPVA Experiment**

The procedures to run the CPVA experiment system are described as follows:

- 1.Clear everything from the test table.
- 2. Make sure safety switch works and you can reach it easily.
- 3. Turn on the FFT analyzer, low pass filter, signal adder, waveform generator and torque transducer amplifier.
- 4. Turn on the MAC computer and run the speed controller.
  - 4.1 Start the LabView and run the 'CPVA' program.
  - 4.2 Turn on the 'SAFETY SWITCH' button on the screen.
  - 4.3 Set the PI controller parameters to:  $K_p=0.12$  and  $K_f=0.08$ .
  - 4.4 Choose the motor mean speed that you want, for example, 300RPM.
  - 4.5 Set the reset button to 'ON' on the screen and the MAC computer speed controller is ready to go.
- 5. Turn on the power switch of the torque controller on the wall. The black controller should be Drive Ready.
- 6. Turn on the "START" and at the mean time, quickly turn the Potential Meter to "100%".
- 7. Push the reset button of the MAC speed controller to 'OFF' and the MAC computer will begin to control the motor mean speed to the value you set. It will take 1-3 minutes to be stable.

- 8. Set the Waveform generator and generate the oscillatory torque signal that you need.
- 9. Use the FFT analyzer to collect the speed and torque signal.

#### **Additional Notes**

- 1. Safety is very important!
- 2. Make sure safety switch is close at hand during the experiment.
- 3. At any sign of emergency, e.g., unknown sound, increased vibration, etc., throw the safety switch or push the red "Stop" button of the torque controller and turn off the power.
- 4. Make sure the Waveform Generator output is correct before you connect it to the signal adder. The amplitude of this signal is normally below 500mV. Be very careful when you alter the amplitude during the experiment when the motor is running.

## **APPENDIX C**

## **CPVA Experiment Devices Calibration**

It's important to calibrate all the devices used in the experiment and make sure they performed as specified. The FFT analyzer and the waveform generator have self-calibration function features and it is a simple matter to independently check these units. Similarly, the operation of the low-pass filter can be easily checked. The calibration of the torque transducer and the frequency-to-voltage converter are described as follows.

#### C.1 Calibration of the torque transducer

The torque transducer is an in-line unit that is coupled to the drive shaft of the motor at one end and has the shaft of the flywheel attached at the other. Torque transmitted through the unit is measured by strain gauges attached to the meter's shaft. Output from the strain gauges are fed to a Measurements System type 2210 conditioning amplifier set with an amplification of 300 and a low-pass filter setting of 100Hz. The amplifier activates the strain gauge with +10 volts. If the reading from the amplifier is  $T_{\nu}(mV)$ , then the manufactures specifications state that the torque will be (allowing for the amplifier setting):

$$T_{\theta} = \frac{T_{\nu}}{300} * \frac{67}{10*1.4562}$$

where  $T_{\theta}$  is the actual torque transmitted by the shaft in Nm units.

We calibrated the torque transducer by installing a 1m steel bar and manually applying a static force that was measured by a force meter. The calibration result shows that the torque transducer and the amplifier works well and that the measured torque value is correct.

#### C.2 Calibration of the frequency-to-voltage converter

The frequency-to-voltage converter can be set to operate over a wide range of frequencies. For our choice of settings, we have the following limitations:

- Minimum Frequency: 3kHz
- Maximum Frequency: 10kHz
- Volts/kHz: 1.00
- Response Time to Reach 99% of Final Value: 10msec

Since the encoder attached to the shaft of the motor outputs 1000pulse/rev., the angular velocity,  $\dot{\theta}$ , can be calculated from

$$\dot{\theta} = 2\pi \frac{\theta_{\nu}}{1000} (rad/s)$$

where  $\theta_{\nu}$  is the output voltage from the frequency-to-voltage converter measured in mV. The accuracy of the converter and the conversion factor were checked by inputting a TTL signals of known frequencies. Also, input frequencies sweeps were

tested at known values to check that the converter would accurately follow the signals.

All checks confirmed the accuracy of the unit.

Table C.1 summarizes the relationship for the torque, speed and acceleration measurements.

Table C.1 Experiment result conversion

Item	Physical	FFT Reading(mV)	Experiment Value		
$T_{\theta}$	Varying applied torque	$T_{\nu}$ (mV)	$T_{\theta} = \frac{Tv}{300} * \frac{67}{10*1.4562} (N*m)$		
$\dot{ heta}$	Rotor angular velocity	$\theta_{v}(mV)$	$\dot{\theta} = 2\pi \frac{\theta_{\nu}}{1000} (rad / s)$		
Ö	Rotor acceleration	$\theta_{v}(mV)$	$\ddot{\theta} = 2\pi f_n * 2\pi \frac{\theta_v}{1000}$		

### APPENDIX D

### Discussion of the CPVA order

In section 4.2.2.2, the measured order of the CPVA is 3.5, which is much larger than the theoretical prediction of 2.5. For this case, the cord length should be 12.9mm instead of the actual length of 25.3mm. To try and understand why this discrepancy exists, many issues were explored.

#### 1. Geometry of the CPVA system

We measured the CPVA dimensions, including shaft dimension, absorber dimension and its center of gravity, and the cord length many times. The results were always identical. Also the position of CPVA path center around which CPVA rotates is determined by geometry.

#### 2. 3-DOF CPVA model

Figure 4.1 shows the system frequency response with the absorbers locked. Clearly an additional DOF is present and so the 3-DOF CPVA model was analyzed in Section 2.2.2. We were trying to see if any change in the shaft stiffness would explain the increase in the measured order of the system. Figure 2.11 shows the result of decreasing the stiffness, while Figure 2.12 shows the result of increasing the damping. Unfortunately, both cause a decrease in the tuning point of the system, not an increase, as was experimentally observed.

#### 3. Different motor mean speed

Figure 4.1 also shows that there is a minimum point in the system frequency response when the absorbers are locked. This minimum point could affect the system behavior if the CPVA's natural frequency was close to this point. So we changed the motor mean speed from 300RPM to 150RPM and repeated the system frequency response experiment with the same experimental parameters. The system frequency response for 150RPM is shown in Figure 4.5. By using the 3-DOF CPVA model, the estimated CPVA order and the required cord length are shown in Table D.1 (recalling that the actual cord length is 25.3mm.

Table D.1 Estimated CPVA order for different motor mean speed

Motor mean speed	Estimated CPVA order	Estimated cord length
300RPM	3.5	12.9mm
150RPM	3.0	17.6mm

The measured CPVA order for 150RPM motor mean speed is better than that for the 300RPM case. However, there is still a considerable error, compared to the theoretical value of n=2.5.

#### 4. Different absorber cord length

We also manually tuned the CPVA order by changing the absorber cord length and experimentally obtained the system frequency response. Figure 4.6 shows the result with a 300RPM motor mean speed and 40.5mm cord length. Table D.2

compares the measured CPVA order for the two different cord lengths. It indicates that there is still a difference between the actual cord length and the theoretically estimated values.

Table D.2 Estimated CPVA order with different absorber cord lengths

Absorber	string	Expected	CPVA	Estimated	CPVA	Estimated	cord
length		order		order		length	
25.3mm		2.5		3.5		12.9mm	
40.5mm		1.98		2.3		29.9mm	

#### 5. Different oscillatory torque form

The 2-DOF CPVA and 3-DOF CPVA models in Chapter 2 are based on the assumption that the applied torque is of the form  $Tsin(\omega t)$ . Experimentally, we can generate this type of torque or one of the form  $Tsin(n\theta)$ . Experiments show that the linear system frequency response curve for these two cases are identical when the applied torque is small, 0.50Nm. While this was not expected to influence the measured order, it does allow us to more quickly complete the experiments since creating  $Tsin(n\theta)$  is more time consuming.

#### 6. Independent data measurements

Shaft speed and torque measurements are available directly from the servo motors drive. They are completely independent of the corresponding signal form the

frequency-to-voltage converter and the torque meter. Using these signals, we repeated the system frequency response experiment. The response curve and the estimated CPVA order didn't change. Also, we doubled checked the frequency-to-analog converter using an independent signal source.

#### 7. Damping model

A 3-DOF model was analyzed that included the rotor damping. The analytical solution shows that the rotor damping didn't change the minimum point position of the system frequency response. Also, we modeled the absorber damping as  $cr(\dot{\theta} + \dot{\phi})$  instead of  $cr\dot{\phi}$ . The system response did not change near the minimum point.

#### 8. Lock one absorber and free the other one

There are two absorbers in our CPVA experimental system. It's hard to difficult the two absorbers identical and so we locked one of them and freed the other absorber and repeated the system frequency response experiment. Experimental results show that the minimum point of the one free absorber is very close to that of the two free absorbers. Plots are shown in Figure D.1.

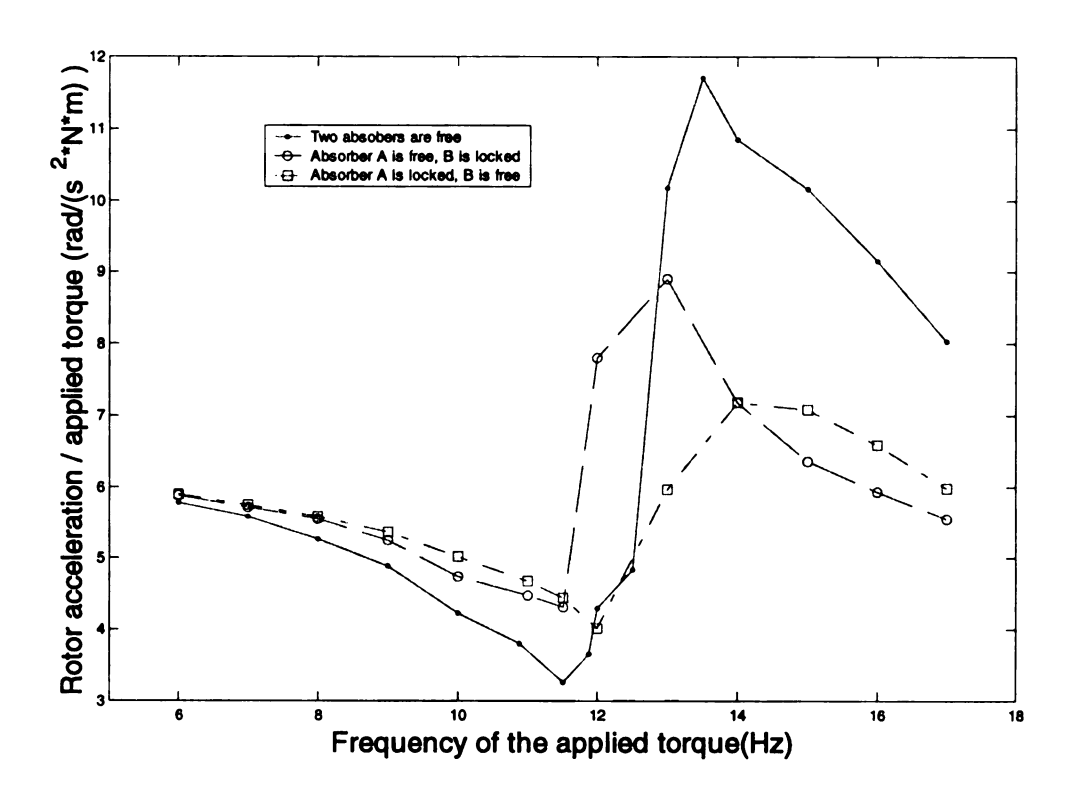


Figure D.1 System frequency response with various absorbers locked/unlocked.

Cord length is 40.5mm and torque level is 0.50Nm.

## **BIBLIOGRAPHY**

#### **BIBLIOGRAPHY**

- A.S. Alsuwaiyan, 1999 Performance, Stability, and Localization of Systems of Vibration Absorbers, PhD thesis, Michigan State University.
- C.P. Chao, 1997 The Performance of Multiple Pendulum Vibration Absorbers Applied to Rotating Systems, PhD thesis, Michigan State University.
- C.P. Chao and S.W. Shaw, paper DETC97/VIB-3956, Proceedings 1997 ASME Design Engineering Technical Conferences. Nonlinear localization in systems of tautochronic vibration absorbers.
- H.H. Denman, 1992 Journal of Sound and Vibration 159, 251-277. Tautochronic Bifilar Pendulum Torsion Absorbers for Reciprocating Engines.
- J.P. Den Hartog, 1938 *Tuned Pendulum as Torsional Vibration Eliminators*. In Stephen Timoshenko 60<sup>th</sup> Anniversary Volume, pages 17-26. The Macmillan Company.
- J.P. Den Hartog, 1956, Mechanical Vibrations, pages 87-92, McGraw-Hill, New York.

Reimund Keiser, 1998, Design, Construction and Testing of an Apparatus for Measuring the Behavior of Torsion Vibration Absorbers, Cand.-Ing thesis, Michigan State Unveristy.

- D.E. Newland, 1964 ASME Journal of Engineering for Industry 86, 257-263. Nonlinear aspects of the performance of centrifugal pendulum vibration absorbers.
- S.W. Shaw, V. Garg and C.P. Chao, 1998 Attenuation of Engine Torsional Vibration Using Tuned Pendulum Absorbers. To appear.
- E.S. Taylor, 1936, Annual Meeting of the Society, Detroit, Jan. 17. Crankshaft Torsional Vibration in Radial Aircraft Engines.